OSE FINAL REPORT
D9.5

Grant Agreement n° 262584
Project Acronym: JERICO

Project Title: Towards a Joint European Research Infrastructure network for Coastal Observatories

Coordination: P. Farcy, IFREMER,

jerico@ifremer.fr, www.jerico-fp7.eu:

Authors: Z. Wan, A. Aydogdu, N. Pinardi, G. Korres, J. Schulz-Stellenfleth, M. Verlaan, J. Sumihar, S. Ponsar
Involved Institutions: DMI, CMCC, HCMR, HZG, DELTARES, MUMM
Version and Date: Version 1.0 Dec 2014

Table of Contents

Document description

REFERENCES

Annex 1 to the Contract: Description of Work (DoW)

Document information	
Document Name	D9.5 - Second report OSE: Task 9.2 - Second report on the results of OSE experiments
Document ID	
Revision	
Revision Date	29 Dec 2014
Author	Z. Wan, A. Aydogdu, N. Pinardi, G. Korres, J. Schulz-Stellenfleth, M. Verlaan, J. Sumihar, S. Ponsar
Security	

History			
Revision	**Date**	**Modification**	**Author**

Diffusion list				
Consortium beneficiaries	X			
Third parties				
Associated Partners				

Introduction

The objective of the second (final) scientific report on Observation System Experiments (Deliverable D9.5) is to assess the impact of existing observational platforms on estimates of coastal processes through the work done within JERICO WP9.2 and thus to contribute to the future strategy for coastal observatories at the coastal scale. To this end, OSE studies can provide valuable information on evaluating the different components of the present-day observing system.The experiments reported here by DMI, CMCC, HCMR, HZG, DELTARES and MUMM are applied in most European coastal areas (Baltic Sea, Adriatic Sea, Aegean Sea and the North Sea) using different 3D circulation models (HIROBM, NEMO, POM, GETM, DCSM, COHERENS) implemented at a high spatial resolution and accompanied by data assimilation systems of different complexity (ranging from Optimal Interpolation to Ensemble Kalman filtering) to blent model solutions with the available observational data sets. In what follows the results of OSE studies are reported for the Baltic Sea (DMI), Adriatic Sea (CMCC), Aegean Sea (HCMR) and the North Sea (HZG, DELTARES & MUMM) using different observing systems ranging from T/S profiles from CTD casts and fixed platforms (Baltic Sea, North Sea), temperature profiles from the Fishing Vessels Observing System (Adriatic Sea), tide gauges (North Sea), HF Radars (North Sea, Aegean Sea) and FerryBox systems (Aegean Sea).

1. OSE in the Baltic – North Sea (DMI)

1.1. Experiment set-up

a) Physical model

In the Baltic Sea, DMI is running a two-way nested, free surface, hydrostatic three-dimensional (3D) circulation model called HIROBM-BOOS (HBM). The model code forms the basis of a common Baltic Sea model for providing GMES Marine Core Service since 2009. The finite difference method is adopted for its spatial discretization in which a staggered Arakawa C grid is applied on a horizontally spherical and vertically z-coordinate.

The model has a horizontal resolution of about 6 nautical miles (nm) and 50 vertical layers. The top layer thickness is selected at 8 m in order to avoid tidal drying of the first layer in the English Strait. The rest of the layers in the upper 80 m have 2 m vertical resolution. In the Danish Strait, the horizontal resolution is increased to 1 nm to better resolve the complex bathymetry. A detailed description of the model can be found in Berg and Poulsen (2011).

The meteorological forcing is based on a reanalysis using the regional climate model HIRHAM through a dynamic downscaling (including a daily re-initialization) from ERA-Interim Global reanalysis. HIRHAM is a regional atmospheric climate model (RCM) based on a subset of the HIRLAM and ECHAM models, combining the dynamics of the former model with the physical parameterization schemes of the latter. The original HIRHAM model was a collaboration between DMI, the Royal Netherlands Meteorological Institute (KNMI) and MPI. A detailed description of HIRHAM Version 5 can be found in Christensen et al. (2006).

b) Data assimilation scheme

A 3DVAR method has been applied to assimilate the satellite SST, in situ temperature and salinity profiles into a coupled physical-biogeochemical model in the Baltic Sea. In general, the basic scheme of 3DVAR is to find the optimal solution of the model state **x** which minimizes the following cost function:

$$J(\mathbf{x}) = \frac{1}{2}(\mathbf{x}-\mathbf{x_b})^T \mathbf{B}^{-1}(\mathbf{x}-\mathbf{x}_b) + \frac{1}{2}(H(\mathbf{x})-\mathbf{y}_o)^T \mathbf{R}^{-1}(H(\mathbf{x})-\mathbf{y}_o) \qquad (1.1)$$

$\mathbf{x}$ is the model state to be estimated. It usually refers to analysis state vector. $\mathbf{x}_b$ is the background state vector, $\mathbf{y}_o$ is the observation state vector. H is the non-linear observational operator with which the analysis equivalent of observation $\mathbf{y} = H(\mathbf{x})$ can be obtained to compare with the observation measurements. The superscript T denotes matrix transpose. In the cost function, the misfit between analysis and background is weighted by the background error covariance **B**, and the misfit between analysis and observation is weighted by the observational error covariance **R**. Usually the optimal solution is found by minimizing the cost function $J(\mathbf{x})$ with respect to $\mathbf{x}$, in which its gradient is also needed for determining the search direction and iteration steps in the minimizing algorithm:

$$\nabla J(\mathbf{x}) = \mathbf{B}^{-1}(\mathbf{x} - \mathbf{x}_b) + \nabla_{\mathbf{x}} H(\mathbf{x})^T \mathbf{R}^{-1}(H(\mathbf{x}) - \mathbf{y}_o) \qquad (1.2)$$

Following an incremental method (Courtie, etc. 1994), Equation (1.1) is linearized around the background state into the following form:

$$J(\delta\mathbf{x}) = \frac{1}{2}\delta\mathbf{x}^T \mathbf{B}^{-1}\delta\mathbf{x} + \frac{1}{2}(\mathbf{H}\delta\mathbf{x} - \mathbf{d})^T \mathbf{R}^{-1}(\mathbf{H}\delta\mathbf{x} - \mathbf{d}) \qquad (1.3)$$

where $\mathbf{d} = \mathbf{y}_o - H(\mathbf{x}_b)$ is the innovation vector, $\mathbf{H}$ is the linearized observation operator evaluated at $\mathbf{x} = \mathbf{x}_b$ and $\delta\mathbf{x} = \mathbf{x} - \mathbf{x}_b$ is the analysis incremental vector. In this way, the original problem converts into finding an incremental analysis $\delta\mathbf{x}$. Equation (1.2) becomes :

$$\nabla J(\delta\mathbf{x}) = \mathbf{B}^{-1}\delta\mathbf{x} + \mathbf{H}^T \mathbf{R}^{-1}(\mathbf{H}\delta\mathbf{x} - \mathbf{d}) \qquad (1.4)$$

In our current scheme, the state vector contains only temperature and salinity model state variables:

$$\mathbf{x} = \begin{bmatrix} T & S \end{bmatrix}^T \qquad (1.5)$$

b) Observation systems

Two observation systems of satellite remote sensing and moorings are examined in the Baltic Sea (Figure 1.1). Black crosses mark the sampling locations of moorings and red crosses stand for the locations of other observations. T/S profiles are measured by CTD instrument.

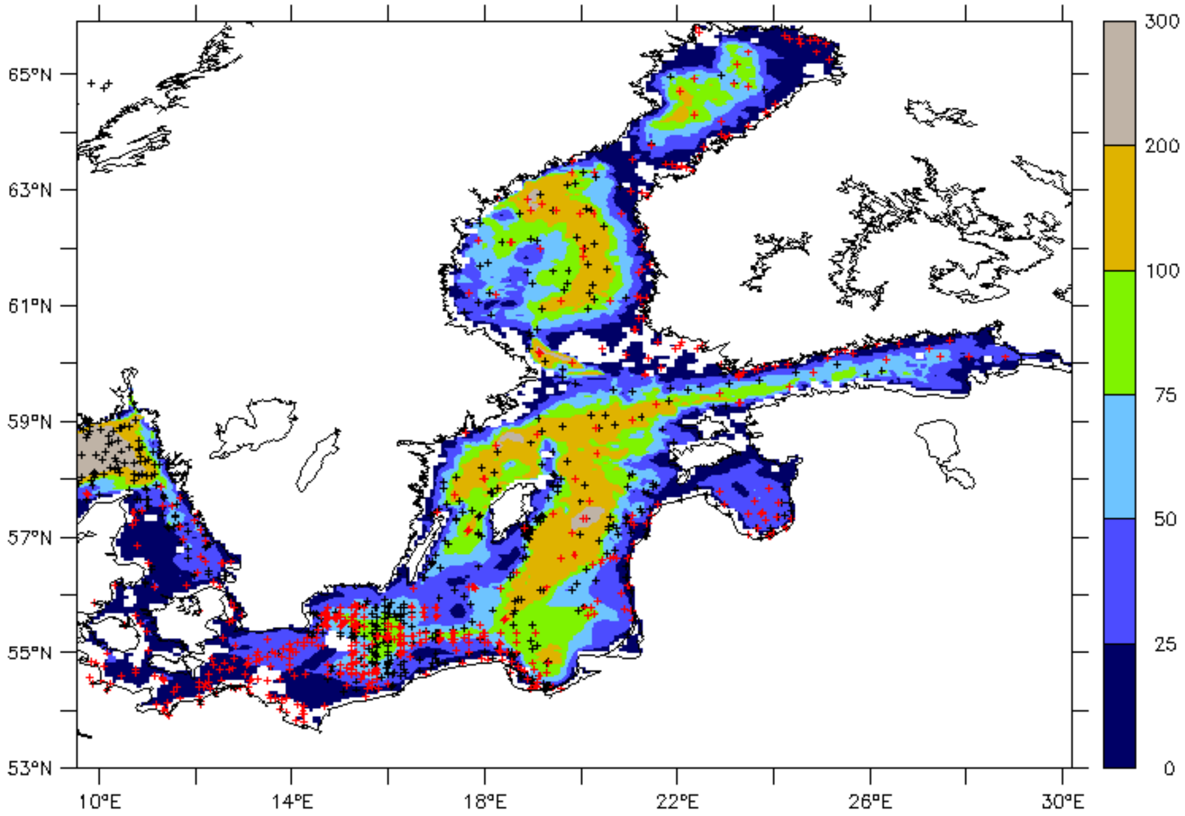

Figure 1.1 Model domain and sampling locations: black crosses for T/S profiles and red crosses for others

c) Experiments

Observation System Experiment (OSE) is used to assess its effect in improving prediction products through data assimilation. OSE is a widely used scheme to assess and to complete existing observation systems. The OSE experiments in the Baltic Sea are described as follows.

Exp. 0: reference run, without data assimilation

Exp. 1: identical to reference run, but assimilating data SST from satellite remote sensing

Exp. 2: identical to reference run, but assimilating data T/S profiles from moorings

Exp. 3: identical to reference run, but assimilating both data SST and T/S profiles.

1.2. Results

a) Temporal evolution of mean deviations from scenarios to observations

Temperature and salinity integrated over entire model domain are compared among four experiments against observations (Figure 1.2). As we can see, changes among four experiments are relatively small. Deviations of four experiment results from observations are depicted in Figure 1.3. It is clear that assimilating data from either observation systems can improve model predictions. The combination of two observation systems works better than individuals.

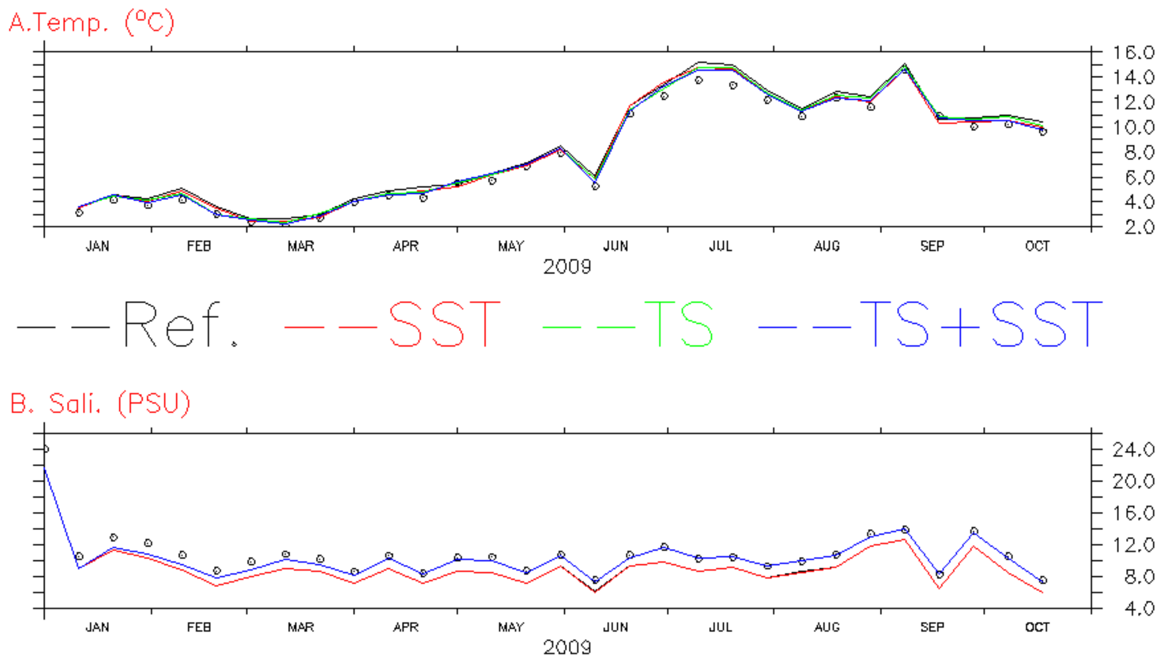

Figure 1.2 Model results of four experiments (colored curves: black, red, green, blue for Exp.s 0-3, respectively) integrated over basin in comparison with observations (black cycles) for temperature (a) and salinity (b).

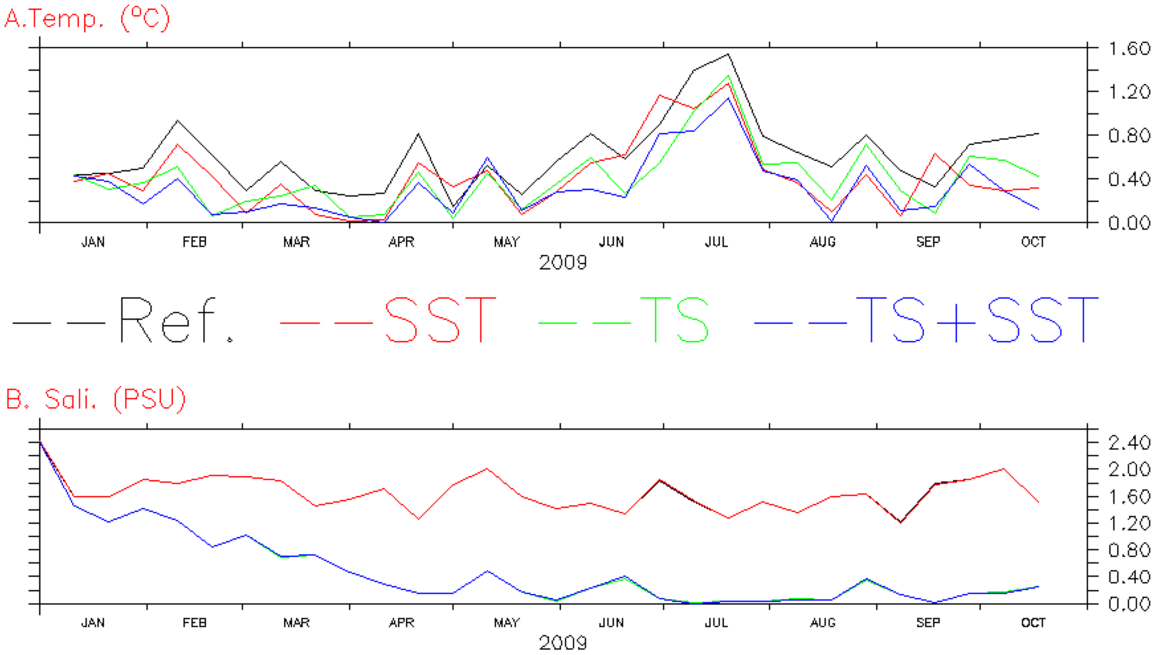

Figure 1.3 Mean deviations of model results from observations for four experiments (colored curves: black, red, green, blue for Exp.s 0-3, respectively) for temperature (a) and salinity (b).

b) Regional distribution of mean deviations and improvements

Regional distribution of mean deviations between model results of Exp. 0 and observations and as well improvements of Exp.s 1-3 relative to Exp. 0 are depicted in Figure 1.4. As we can see (Panels a & e), the mean model deviations for both temperature and salinity are smaller in Danish Straits and Southern Baltic Sea than in other regions. Except for a few spots of minor negative impacts (Panels b-d), positive improvements for temperature are apparent in each data assimilation experiments. Assimilating SST data doesn't improve model prediction on salinity so that prediction improvements are nearly identical in Exp.s 2 & 3.

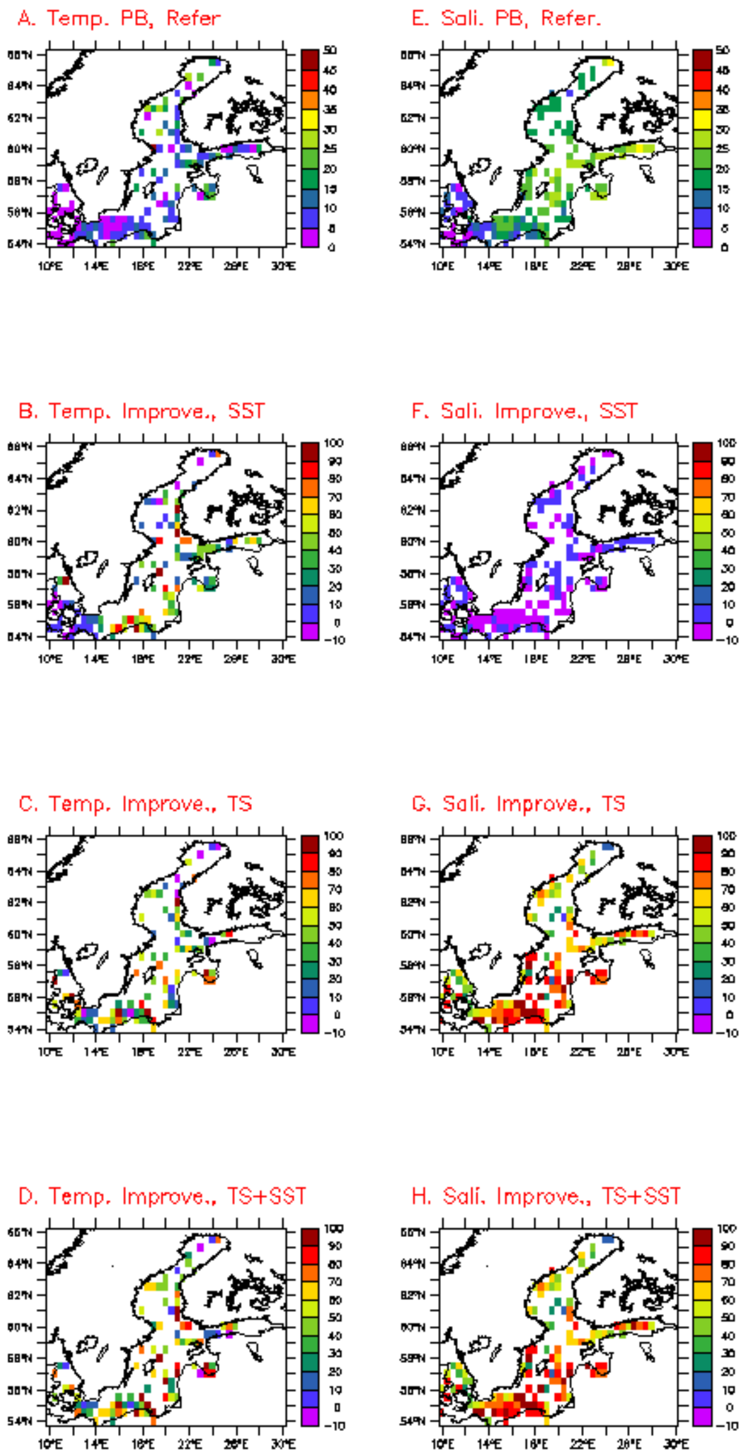

Figure 1.4 Regional distribution of percentage deviations between prediction products and validation data. Panels in left (right) for temperature (salinity), panels in first row for absolute percentage deviations in reference run (a & e), panels in other rows for percentage improvements relative to reference run as to assimilating data SST (b & f), T/S profiles (c & g) and SST + T/S (d & h).

d) Results in statistics

Statistics based on all observed bins show that the fitness of temperature between model predictions and observations in the reference run (Exp. 0) is 0.91, 0.10, 0.89 and 7.1% in terms of determination coefficient (R^2), cost function (CF), model efficiency (ME) and percentage bias (PB), respectively (Table 1.1), and the fitness for salinity is 0.95, 0.11, 0.90, -16% in terms of metrics R^2, CF, ME and PB, respectively (Table 1.2). The improvements of data assimilation are calculated in percentage changes relative to the reference run. As we know, larger values of R^2 and ME mean better fitness between model predictions and observations, but smaller values of CF and PB mean better fitness. Thus the percentage changes standing for improvements are calculated for R^2 and ME in the way opposite to for CF and PB.

Table 1.1 Statistical metrics for the fitness between prediction products and validation data for temperature

Temperat.	**R^2**	**CF**	**ME**	**PB**
Refer.	0.91	0.10	0.89	7.1
SST	+0.2%	+7.9%	+1.2%	+45%
TS	+1.9%	+22%	+2.8%	+32%
TS+SST	+2.1%	+25%	+3.4%	+49%

Table 1.2 Statistical metrics for the fitness between prediction products and validation data for salinity

Salinity	**R^2**	**CF**	**ME**	**PB**
Refer.	0.95	0.11	0.90	-16.
SST	+0.00%	+0.00%	+0.00%	-0.03%
TS	+1.6%	+61%	+6.9%	+73%
TS+SST	+1.6%	+61%	+6.9%	+73%

1.3 Discussion and lessons learnt

In this study, OSEs are performed for investigating the impacts of the existing Baltic Sea observation systems based on satellites (sea surface tenperature) and moorings (temperature and salinity profiles). It was found that significant error reductions can be archived by assimilating the data into the DMI ocean-ice coupled model. In terms of determination coefficient (R^2), cost function (CF), model efficiency (ME), assimilating T/S profiles results significantly better results of 3D water temperature than assimilating satellite SST while the latter performs better regarding the percentage bias (PB). The combination of both observation systems can improve prediction products more than individuals. Results also show that assimilating SST doesn’t visibly impact on salinity.

2. OSE in the Adriatic Sea (CMCC)

2.1 Introduction

2.1.1 Geographical Setup

The Adriatic Sea is located in the northern part of the Central Mediterranean, between the Italian peninsula and the Balkans. It has a highly variable depth varying from about 30 m in the Northern Adriatic to 1200 m in the Southern Adriatic (Fig. 2.1). It is connected to the Mediterranean Sea through Otranto Strait. The Adriatic Sea is characterized by a large spatial variability of the atmospheric forcing, inducing large seasonal thermohaline and circulation variations, and the river discharge. In particular the large river discharge exceeds the evaporation and determines the estuarine exchange with the Mediterranean Sea. The near surface circulation is mainly cyclonic with a permanent South Adriatic Cyclonic Gyre and a Middle Adriatic Cyclonic Gyre. The Mediterranean water inflows along the eastern coast, and the permanent Western Adriatic Coastal Current flows southward, driven by both the salinity gradient due to the large river run-off at the northern coasts and the winds. The dense water generated during the winter in the Adriatic Sea outflows through the lower layer of the Otranto Strait and represents a significant source of dense waters in the Eastern Mediterranean.

1.2 Model Description

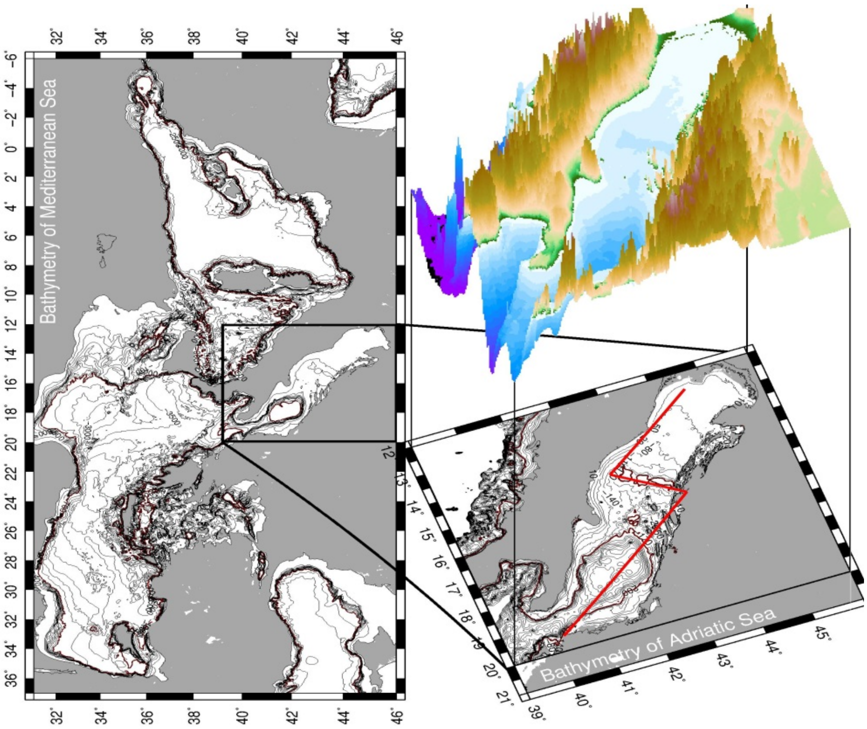

Fig. 2.1: Adriatic Sea Geometry and Bathymetry. The red line indicates the section for vertical field visualization.

The numerical model set-up in the Adriatic Sea has a constant grid resolution of 1/48° along the longitudinal

and latitudinal directions that corresponds to 1.8 and 2.3 km respectively and it uses the NEMO (Nucleus for European Modeling of the Ocean, Madec, 2008) code in its explicit free-surface formulation. The model grid has 432 points in the zonal, and 331 in the meridional direction. In the vertical direction, it is configured with 120 unevenly spaced horizontal z-levels. The bottom topography is represented by the partial cell method. Vertical grid spacing is 1 m in the top 60 m, then increases to 9 m at 100 m depth and further to 50 m at the deepest point in the Adriatic Sea. The largest spacing of 70 m is in the Ionian Sea at the deepest point (2800 m). This configuration of the model has been described in a recent paper (Gunduz et al., 2013) and in this work we have used the restart from the published 10 year simulation in January 2007.
Atmospheric forcing fields, except for precipitation, were obtained from the European Centre for Medium-Range Weather Forecasts (ECMWF) ERA-Interim data set. The precipitation was obtained from the Merged Analysis of Precipitation (CMAP) observational data set (Xie and Arkin 1997). The ERA-Interim atmospheric forcing fields are available at the frequency of 6 hour and the horizontal resolution of 0.25°. The monthly mean CMAP data set has the horizontal resolution of 2.5°.
The model set-up has one open boundary communicating with the Mediterranean Sea positioned south of the Otranto Strait (see Fig. 2.1). The boundary conditions for temperature, salinity, sea surface height, zonal and meridional current are provided daily from the large scale MFS Mediterranean Forecasting System (Pinardi and Coppini, 2010).

2.1.3 OceanVar Data Assimilation System

The system consists of the Adriatic set-up of the NEMO ocean model described above and the OceanVar data assimilation scheme (Dobricic and Pinardi 2008). In the OceanVar set-up the slowly evolving vertical part of temperature and salinity background error covariances is represented by monthly varying Empirical Orthogonal Functions (EOFs). They are calculated in each model point separately by the method described in Dobricic et al. (2006).
The horizontal part of background error covariances is assumed to be Gaussian isotropic depending only on distance. It is modeled by the successive application of the recursive filter in longitudinal and latitudinal directions, that provides a high computational efficiency in each iteration of the algorithm. The rapidly evolving part of the background error covariances, consisting of the sea level and the barotropic velocity components is modeled in each step of the minimization algorithm by applying a barotropic model forced by the vertically integrated buoyancy force resulting from temperature and salinity variations. The velocity is then estimated by applying the geostrophic relationship, modified along the coast by the application of the divergence dumping filter in order to eliminate the horizontal divergence. In this way OceanVar combines long term three dimensional variational scheme for the slow processes with a scheme that fully dynamically evolves the covariances by model equations for the fast processes. In particular the dynamical model used for the simulation of covariances between sea level errors and errors in temperature and salinity fields allows their very accurate estimate over areas with highly variable or shallow bottom topography typical for coastal areas.

2.1.4 Fishery Observing System

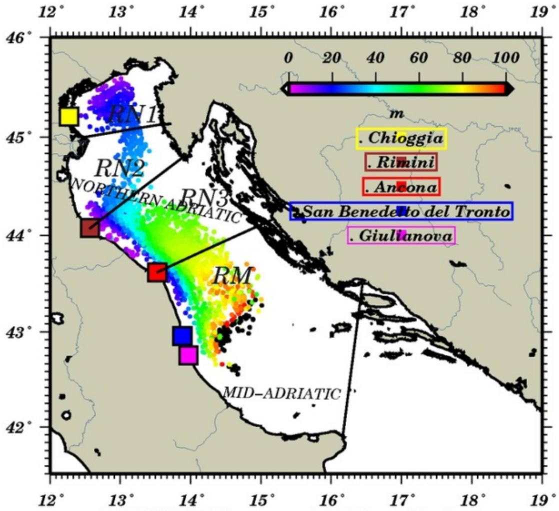

ADRIATIC SEA Sections and FOS Depth Distribution

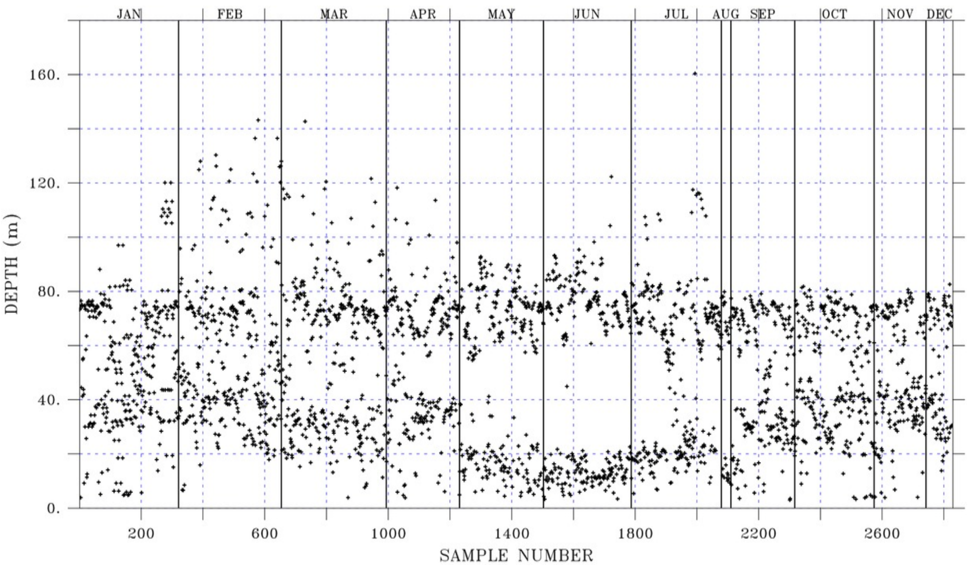

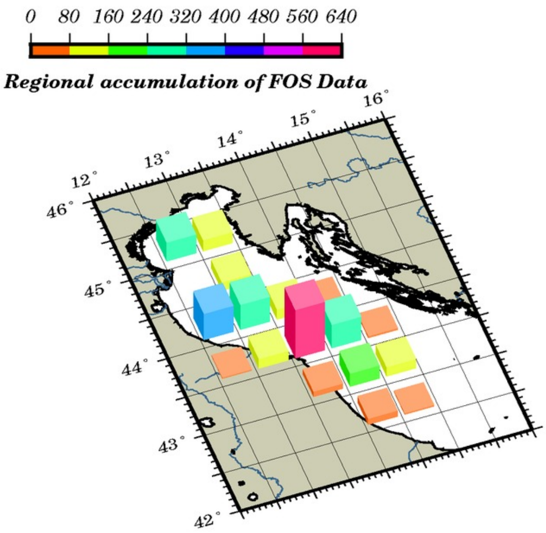

Fig. 2.2: The depth distribution of the FOS data and regional subdivision of the Adriatic Sea (top panel). Depth of the measurement caluclated as an average of the net fishing depth (middle panel). Horizontal monthly cumulative distribution of the measurements (bottom

During JERICO, the Observing System Experiments (OSE) assimilate observations, provided by CNR partner, from the voluntary fishing vessels monitoring system (Fishing Observing System, FOS). The FOS data used in this study consists of seven different vessels from five different fleets in 2007. Fleets are located in Chioggia, Rimini, Ancona, San Benedetto del Trento and Giulianova from north-west to mid-west Adriatic Sea, respectively. StarOddi sensors are installed to the nets of the pelagic pair trawlers and purse seine fishing vessels. Sensor measures temperature with an accuracy of ± 0.1°C. Depth is calculated from pressure which has an accuracy ± 0.4% with the selected range for 50m-270m range. Profiles taken during the releasing and hauling of the net is excluded from the assimilation experiments due to the stabilization problem of the sensor. Moreover, the horizontal profile taken during the net drift is averaged along the track. As a result, the dataset used in the assimilation consists of point data well-distributed along the Italian side of the northern and middle Adriatic Sea (Fig. 2.2).
The measurement points reach a maximum depth of 160m but most of them stay within the first 100 m. Largest amount of data is collected by the Ancona and Rimini fleets. There were two vessels in those fleets whereas only one vessel was available in each of the other fleets. Least amount of data is collected during August due to the restrictions on fishing activities (Fig. 2.2).

2.2 Design of the Observing Simulation Experiments (OSE)

The OSE are designed to show the impact of FOS on the quality of the analysis with respect to simulations and to check the impact of a reduced number of fishing vessels on the analysis quality. All experiments are listed in Table 2.1.

NAME	TYPE	ASSIMILATION
CONTROL RUN	SIMULATION	NO
BEST ESTIMATE	ASSIMILATION	ALL FOS
OSE01	ASSIMILATION	SELECTIVE FOS 4 Vessels
OSE02	ASSIMILATION	SELECTIVE FOS W/O Ancona

NAME	CHIOGGIA	RIMINI	ANCONA	Giulianova	San Benedetto
CONTROL RUN	0	0	0	0	0
BEST ESTIMATE	1	2	2	1	1
OSE01	1	1	1	1	0
OSE02	1	2	0	1	1

Table 2.1: OSE characteristics

A control run is performed without assimilation (Table 2.1). Then all of the observations are assimilated to produce an analysis or 'best estimate'. Two other experiments are designed: the first, OSE01 uses only 4 vessels while OSE02 neglects completely the Ancona Fleet.
More specifically in OSE01 the observations collected by one of the two fishing vessels from Ancona and Rimini fleets are excluded. Moreover, the observations from the San Benedetto fleet is not used since it is close to the Giulianova fleet. At the end, OSE01 is performed with four vessels to assess the impact of observations covering all regions of the 2007 system but with less number of vessels.
Almost half of the data are provided by Ancona and Rimini fleets. Moreover, most of the data collected by Ancona fleet is under 30 m depth which is approximately the depth of the surface Ekman layer and also the T,S mixed layer. Therefore, OSE02 is performed without using the Ancona data to evaluate the impact of relatively shallow observations.

2.3 OSE Results

The OSE will be intercompared computing Root Mean Square Errors (RMSE) between model and observations. For the best estimate run and OSE01 and OSE02 the RMSE is calculated from misfits that are the difference between the model background fields before the data have been assimilated and the observations. RMS errors are calculated during post-processing within the layers 0-20 m, 20-50 m and 50-100m depths.

Monthly RMSE of the control run is largest during the stratification season (May to September) in the surface and subsurface layers, as expected (Fig. 2.3). The smallest errors are in the layer between 50 m and 100 m where the water column is generally mixed all the year long. The RMSE varies between 0.6°C (winter) and 2.6°C (summer) in the upper layers and in the sub-thermocline it is around 0.5°C for the whole 2007 period.

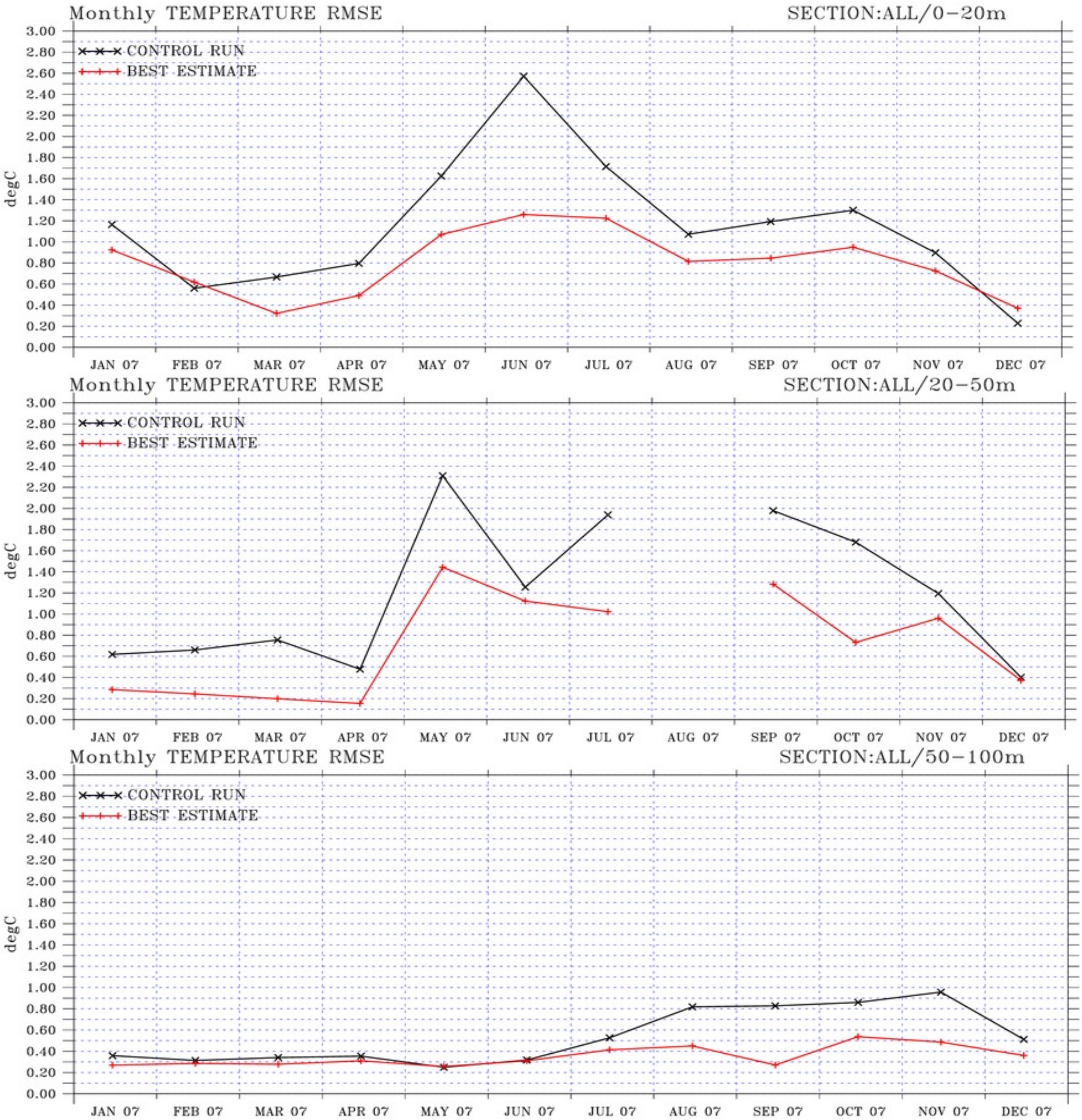

Fig. 2.3: The monthly RMSE of control run (black) and best estimate (red) at 0-20 m, 20-50 m, and 50-100 m from top to bottom, respectively.

The best estimate run that assimilates the data shows an improvement of the RMSE, reducing it to about 50% with respect to the simulation one, except during the winter where it is already low. Thus it can be concluded that FOS can imporve the quality of the best estimates with respect to simulations. The FOS impact is bigger between May and October when the stratification occurs in the first 50 meters. Below 50 meters, the correction become effective only from July to the end of the year.

OSE01 RMSE (Fig. 2.4) show that the impact of decreasing to four fishing is neglegible. This is reasonable since the four vessels sample approximately the same horizontal areas (not shown) as the full fleet (Fig. 2.1), only with fewer repeated mesurements.

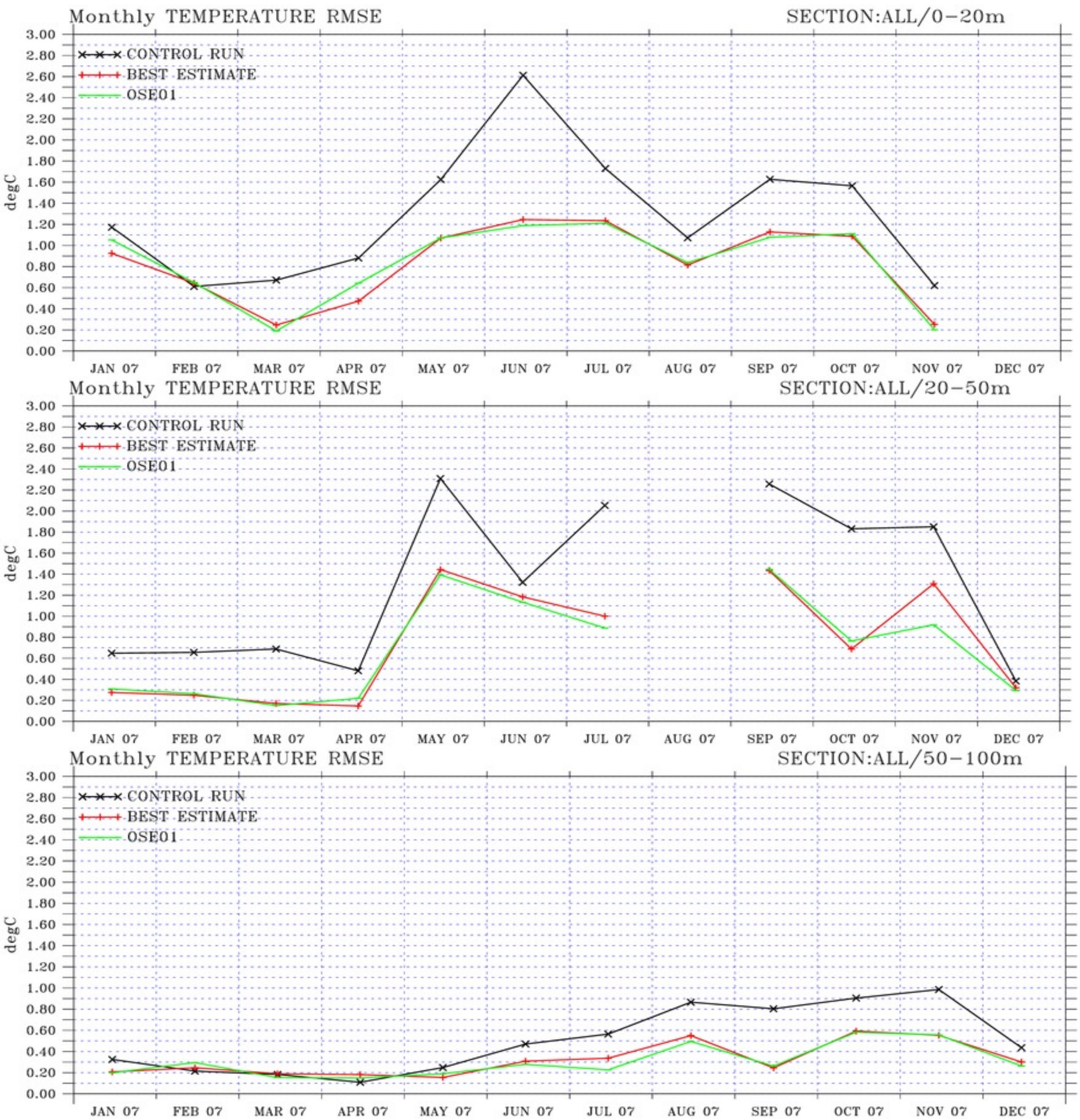

Fig. 2.4: The monthly RMSE of control run (black), best estimate (red) and OSE01 (green) at 0-20 m, 20-50 m, and 50-100 m from top to bottom, respectively.

OSE02, which excludes the observations provided by the Ancona fleet, has again a RMSE similar to the best estimate (Fig. 2.5).

Our results indicate that halving the number of vessels, leaving the coverage unaltered, and decreasing the number of measurements does not have a critical impact on the quality of the analyses. More studies should be carried out to check the importance of each single fishing fleet on the quality of the analyses. However our work confirms for the first time that FOS improves the RMSE by a factor of approximately 50% with respect to the RMSE of the simulation. Our conclusion is then that FOS is an important upper thermocline intensified monitoring system that can provide a tangible improvement in the accuracy of estimating the sea state both in coastal and deep ocean regions.

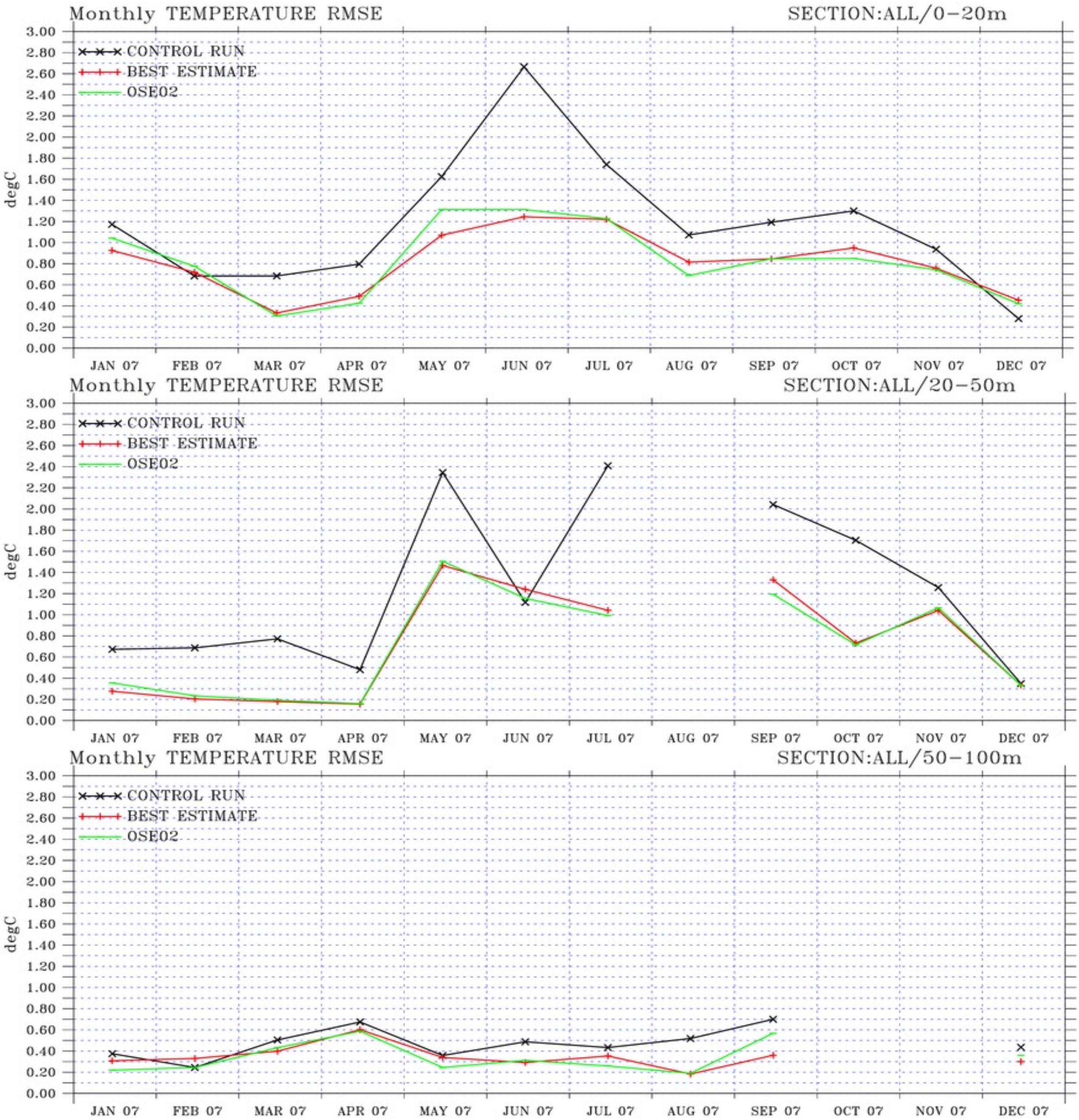

Fig. 2.5: The monthly RMSE of control run (black), best estimate (red) and OSE02 (green) at 0-20 m, 20-50 m, and 50-100 m from top to bottom, respectively.

3. OSE in the Aegean Sea (HCMR)

3.1. Experiment set-up: Model, observations, time of integration, differences between experiments.

The system under consideration in this report includes two observing platforms an HF Radar and a FerryBox system that provide on a regular basis observational data, surface currents between the island of Lemnos and the Dardanelles exit and SST observations along the FerryBox track from Pireaus to Heraklion respectively, the Aegean Sea hydrodynamic model and a filter algorithm that produces an analysis of the model fields by synthesizing the background information the observations and the evolving error statistics.

3.1.1 The hydrodynamic model

The Aegean Sea model is based on the Princeton Ocean model (POM) and was developed as part of the Poseidon system. The model domain covers the geographical area 19.5^{o}E – 30^{o}E and 30.4^{o}N – 41^{o}N (Fig. 3.1) with a horizontal resolution of 1/30^o and 25 sigma layers along the vertical with a logarithmic distribution near the surface and the bottom. The model is forced with hourly surface fluxes of momentum, heat and water provided by the Poseidon - ETA high resolution (1/10^o) regional atmospheric model (Papadopoulos et al., 2002) issuing forecasts for 72 hours ahead. In the Aegean Sea model the Dardanelles inflow/outflow is parameterized as an open boundary where a two layer system is explicitly prescribed with inflow of fresh Black Sea Water (BSW) in the upper layer and outflow of saline Aegean waters below. Additionally, the model includes parameterization of the main Greek rivers Axios, Aliakmonas, Nestos and Evros.

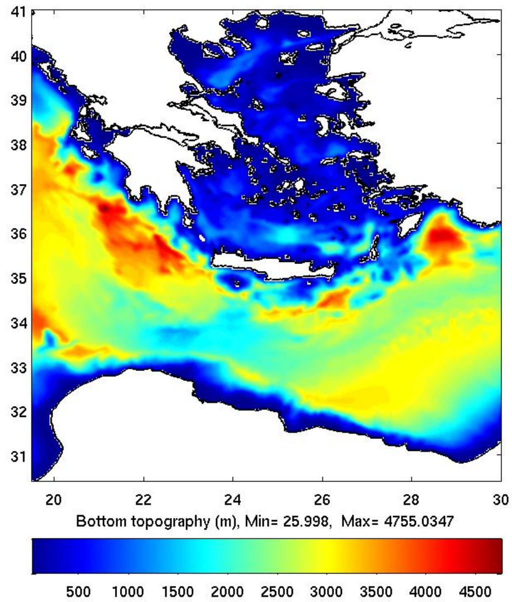

Figure 3.1: The Aegean Sea model bathymetry

Boundary conditions at the western and eastern open boundaries of the Aegean Sea hydrodynamic model are provided on a daily basis (daily averaged fields) by the MyOcean Mediterranean Forecasting System based on NEMO model code and covering the whole Mediterranean basin with a resolution of 1/16^{o} and 72 levels in the vertical. The nesting between the two systems involves the zonal/meridional external (barotropic) and internal velocity components, the temperature/salinity profiles and the free surface elevation following the nesting procedures described in Korres and Lascaratos (2003). Additionally, volume conservation constraints between the two models are applied at both open boundaries of the Aegean Sea model.

3.1.2 The assimilation system

The assimilation scheme used by the Aegean Sea forecasting system, is based on the Singular Evolutive Extended Kalman (SEEK) filter which is an error subspace extended Kalman filter that operates with low-rank error covariance matrices as a way to reduce the prohibitive computational burden of the extended Kalman filter (Pham et al., 1997). The filter is additionally implemented with covariance localization and partial evolution of the correction directions (Korres et al., 2010).

In the standard operational run of the Aegean Sea forecasting system and all assimilation runs performed here, the rank of the filter error covariance matrix is set to 60. A higher rank of the error covariance matrix did not lead to any significant improvement in the filter behavior. After several sensitivity assimilation runs, the first 10 modes were allowed to evolve with the tangent linear model while the rest of the modes were kept invariant. In order to localize the filter, we have chosen an influence radius of 200 km outside of which the correlations were set to zero. A further decrease of the radius of influence used for the covariance localization may in some cases introduce dynamically imbalanced structures in the analysis state which subsequently can trigger instabilities in the model. In order to establish the filter error statistics, the Aegean Sea model was first integrated for one year period (September 2007 – September 2008) re-initialized on a weekly basis from the MFS model analysis and forced with the ETA 1/20^{o} atmospheric model analysis in order to sample a set of 366 daily model realizations. This set of model outputs is used to determine multivariate EOFs needed for the initialization of the SEEK filter.

3.1.3 The observations

Observations used by the standard operation cycle of the Aegean Sea forecasting system

The standard assimilation system for the Aegean Sea model inserts on a weekly basis AVISO gridded (1/8^{o}) absolute dynamic topography (ADT) observations for the Aegean Sea area, gridded (1/16^{o}) AVHRR SST data, T/S ARGO profiles and temperature profiles from any available XBTs over the area, using the time evolving filter statistics and the model forecasts in order to estimate the innovations. The AVISO gridded maps of absolute dynamic topography are produced by merging all available satellites into one regional product available at near real time for the Mediterranean Sea.

The WERA HF Radar observations

Daily averaged surface currents over year 2010 from the WERA HF radar system installed at the eastern coast of the island of Lemnos (figure 3.2a) are used in order to examine their effect on the estimation of the hydrodynamic state of the Aegean Sea.

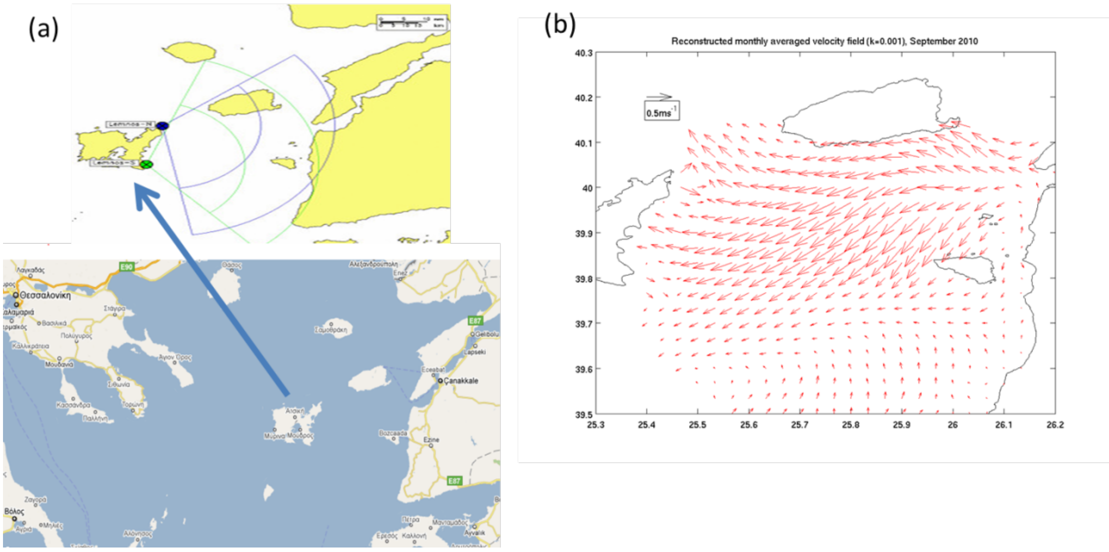

Figure 3.2: a) Setup of the HF Radar system over the eastern coast of Lemnos island b)Monthly mean (September 2010) surface currents distribution measured by the HF WERA system (after reconstruction with OMA method)

The method for processing High Frequency (HF) radar measurements from the WERA radar site in Lemnos Island, Greece, is the Open-boundary Modal Analysis (OMA) in combination with the Nearest Neighborhood Statistics (NNS) method. We applied both techniques to half-hourly surface current data before forming daily-averaged fields for the whole 2010.

Nearest-neighbor Statistics (NNS): "Nearest-neighbor" statistics are used to screen the half-hourly surface currents from the HF Radar for potential errors. A detailed description of the method is given in http://bml.ucdavis.edu/boon/pdf/MethodsPaperHalle.pdf. The NNS method uses a blend of temporal derivatives and spatial comparisons to quantify the acceptability of a given current measurement. Distances to the nearest valid measurements, angular differences between a given current measurement and currents measured nearby, magnitude differences are all used to flag currents as either acceptable or unacceptable. The temporal statistics are based on specifying a time window that is shorter than the typical timescale of system coverage fluctuations (in our case a window of 4 hours was chosen). A sliding window is used to calculate percent coverage statistics at each gridded location (a sliding window of 8 hours was chosen here). Forward and backward in time derivatives of current velocity are also calculated. Currents that change rapidly are removed. The spatial statistics are based on proximity and current differences. Distances from a given current measurement to the nearest 3 (or 5 or 10) gridded locations with valid current measurements are used as a basis for screening and differences in both current speed and direction between the gridded measurement of interest and its neighbours are calculated. Measurements above user-defined thresholds are removed.

Open-boundary Modal Analysis (OMA): The Open-boundary Modal Analysis method used here follows the procedure described in LEKIEN et al. (2004). The general idea of OMA is to generate a set of modes for a given domain which can be used to approximate any current field on that domain. The amplitudes of those modes are then fit to current measurements inside the domain. The modal series approximation is determined by minimizing a cost function to find the ideal combination of the modes, which gives the best fit to available measurement data. These modes depend only on the shape of the domain. Once they are calculated, they can be stored for repeated use on the same domain.

As an example of the finally processed surface currents data measured by the HF Radar system, in figure 3.2b we show the monthly mean surface currents corresponding to May 2010.

The FerryBox SST data

The FB system average data sampling rate is set to 1 min, along Piraeus (37° 58′N 23° 38′E) to Heraklion (35° 20′N 25° 10′E) route (fig. 3.3). The “Olympic Champion” travels the 165 miles distance at a speed of 20 knots/h collecting 430 samples on average. The trip duration is ~9h and the FB is geographically initiated to log over the 200m isobath, 6 miles north of Heraklion and stops 4 miles south of Piraeus at a depth of 100m. Scheduled routes are performed once a day, during night, with the exception of July and August, the peak tourism season months, when daily cruises are also added on the program. Although the ship track is rather stable, currents, winds and traffic can affect it. Particularly in Saronikos Gulf two distinct tracks exist due to ship traffic regulations. To date, bad weather conditions and FB computer malfunction are the major reasons for missing data. The SST data sampled by the FB are available on a daily basis along the ferry route from Piraeus to Heraklion (or vice versa). The ferry leaves the port (either Piraeus of Heraklion) at approximately 19:00 – 20:00 local time and the route is usually completed within 8-9 hours. The FB data are assumed to be concurrent when assimilated into the model (at 00:00 UTC) - a fair approximation considering the suppressed SST daily cycle. Pre-processing of raw FB data before assimilation involves a routine quality control check using seasonal climatology SST values for the area.

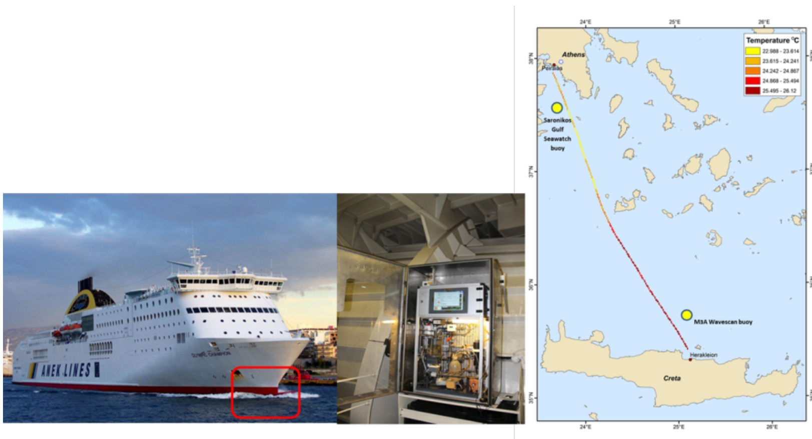

Figure 3.3: The study area with the temperature distribution along the FerryBox track (right) along with the Olympic Champion H/S Ferry hosting the FerryBox station in the bow department (left).

3.2. Discussion on the results

3.2.1 The assimilation of HF Radar surface currents into the Aegean Sea model.

The data assimilation OSE study using the surface currents from the HF Radar system extends over the period May – December 2010 where an almost continuous set of daily surface currents fields area available in the area between the eastern coast of Lemnos island and the Dardanelles Straits. In order to assess the impact of the surface current measurements from the HF Radar system, we have performed four sets of experiments as shown in Table 3.1.

Table 3.1: Description of the different experiments performed with the Aegean Sea model over the period 05.04.10 – 31.12.10

Experiment	Period of model integration	Observations	Frequency of data assimilation
EXP0	05.04.10 – 31.12.10	Satellite SSH-SST and T/S ARGO profiles	Weekly
EXP1	05.04.10 – 31.12.10	Satellite SSH-SST and T/S ARGO profiles. Zonal and meridional surface velocity components from HF Radar	Weekly
EXP2	05.04.10 – 31.12.10	Satellite SSH-SST and T/S ARGO profiles. Zonal surface velocity components from HF Radar	Weekly
EXP3	05.04.10 – 31.12.10	Satellite SSH-SST and T/S ARGO profiles. Meridional surface velocity components from HF Radar	Weekly

EXP0 refers to the standard integration of the Aegean Sea model over the period May – December 2010. In this setup the model assimilates on a weekly basis gridded satellite data of SSH & SST and all available ARGO T/S profiles. Standard model performance is discussed in Korres et al., 2010. In EXP1, the model additionally to the standard set of observations of EXP0 assimilates every week the daily averaged zonal and meridional surface velocity components measured by the HF Radar System. EXP2 considers only the zonal component of the surface currents while EXP3 assimilates only the meridional component. The performance of the assimilation system is assessed by the standard statistic of the RMS error with respect to SSH, SST and the daily averaged surface velocity fields (in the area between the Lemnos island and Dardanelles). On a weekly basis as we consider the model RMS error with respect to observations just before their insertion into the system (forecast RMS error) these observations can be considered as quasi-independent. This is done for the sea surface height. For the surface velocity data the RMS error is calculated on a daily basis and for those dates coinciding with assimilation days the error is calculated before their insertion into the model. Thus the surface velocity can be considered as an independent set for model validation.

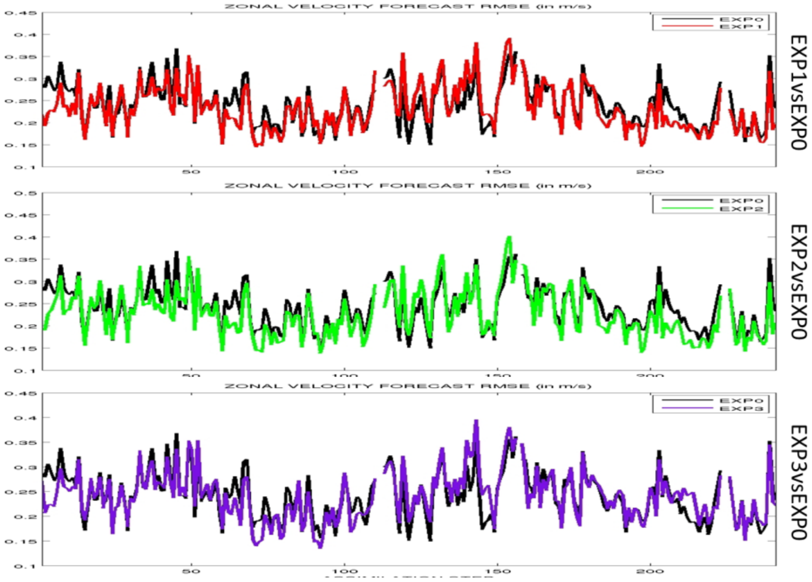

Figure 3.4: RMS error (in m/s) with respect to daily averaged zonal velocity for the period 4 May – 31 Dec 20120. Upper panel: EXP1 (red) vs EXP0 (black), Middle panel: EXP2 (green) vs EXP0 (black) and Lower panel: EXP3 (blue) vs EXP0 (black)

Figure 3.4 presents the temporal evolution of the RMS error (on daily basis) of the zonal surface velocity component for experiments EXP0, EXP1, EXP2 and EXP3. The results obtained in EXP1 and EXP2 clearly show that the introduction of the total or the zonal component of the velocity field between Lemnos and Dardanelles exit leads to a net reduction of the RMS error with respect to the control experiment (EXP0). During the period from mid-August up to the end of September 2010 the insertion of total or zonal velocity data seems to increase in many cases the error with respect to the standard run of the model. On the other hand the assimilation of the meridional component of the surface current alone (EXP3) improves marginally the RMS error from the beginning of the experiment up to mid-August 2010.

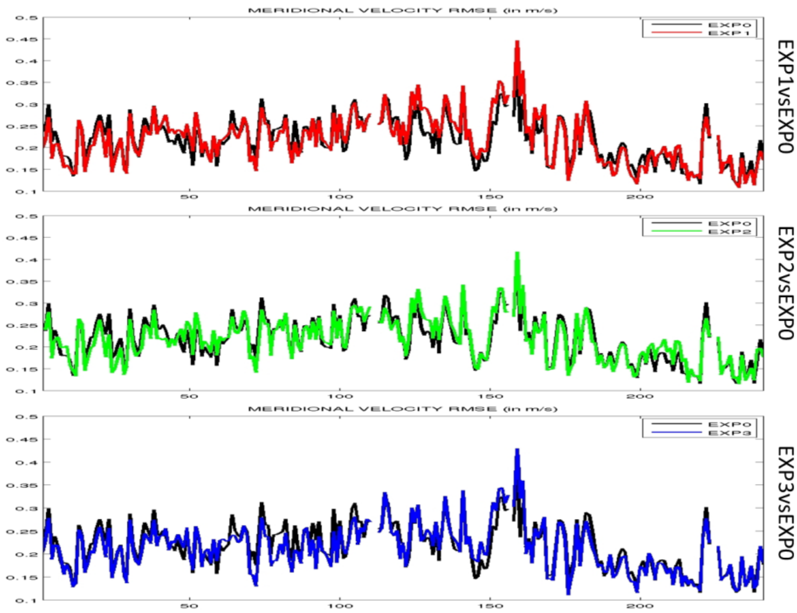

Figure 3.5: RMS error (in m/s) with respect to daily averaged meridional velocity for the period 4 May – 31 Dec 20120. Upper panel: EXP1 (red) vs EXP0 (black), Middle panel: EXP2 (green) vs EXP0 (black) and Lower panel: EXP3 (blue) vs EXP0 (black)

In figure 3.5 we show the temporal evolution of the RMS error with respect to the daily averaged meridional component of the surface current. The assimilation of both components of the surface currents from the HF Radar increases slightly the RMS error for the late summer – early autumn period with respect to the control run. As can be seen by the RMS error corresponding to EXP2 and EXP3 (middle and lower panel of fig. 3.5) this increase is mainly due to the assimilation of the meridional component itself which seems to be dynamically incompatible with what the model predicts at the surface especially during the late summer period.

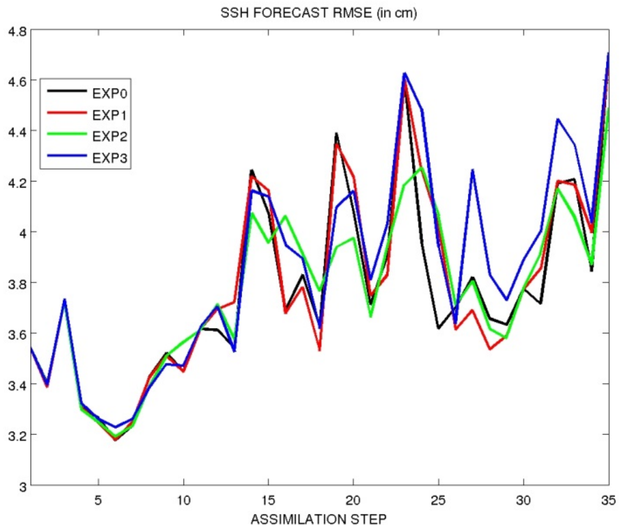

Figure 3.6: SSH forecast RMS error (in cm) calculated on a weekly basis (i.e. at each assimilation time step) for the four experiments.

Finally in figure 3.6 we examine the effect of the assimilation of surface velocity components to the forecast RMS error of the sea surface height over the whole model domain. It is very encouraging that EXP2 (additional assimilation of the HF Radar zonal surface component) implies noticeable changes to the SSH RMS error behavior with respect to the control run (EXP0). This error reduction can be explained on the fact that the correction of the Dardanelles outflow introduced by the assimilation of the HF Radar surface currents data into the model induces changes to the surface circulation field in the North Aegean and secondarily to the rest of the Aegean Sea. These changes are then depicted into the SSH field leading to a decrease of 1 – 1.5 cm for certain periods. For the other two experiments, EXP1 shows some marginal improvement with respect to EXP0 while EXP3 (assimilation of the meridional component) deteriorates the behaviour of the SSH error from assimilation step 27 onwards.

The main result of this study is that the assimilation of the zonal component of the surface currents exiting from the Dardanelles Straits, is beneficial for the Aegean Sea model state estimation. The positive effect of the assimilation exercise is evident in observed and not observed model variables like the meridional component of the surface currents in the area between Lemnos and Dardanelles and the sea surface height. To show in more detail the effect of assimilation of the HF Radar zonal surface currents on the model SSH, we inter-compare in fig. 3.7 the SSH model solution for 07 September 2010 for EXP0, EXP2 with the SSH from satellite altimetry. It is evident that the assimilation of the zonal surface currents changes significantly the distribution of SSH in the North Aegean Sea with accompanied modifications to the circulation field (not shown). North Aegean Sea dynamic features like i) the Thermaikos gulf anticyclonic eddy, ii) the extended anticyclone to the north-west of Lemnos island extending over the Samothraki island and iii) the Skyros anticyclone are correctly depicted in EXP2 results and are totally missing or misplaced in the control experiment. Considering that the Black Sea waters outflowing from Dardanelles Straits follow a cyclonic path within the Aegean Sea flowing southwards along the Greek mainland coastline, we clearly see how the corrections introduced locally in the Dardanelles area propagate and produce a better analysis in remote areas like the outer area of the Saronikos Gulf which is usually affected by the brackish waters of Black Sea origin.

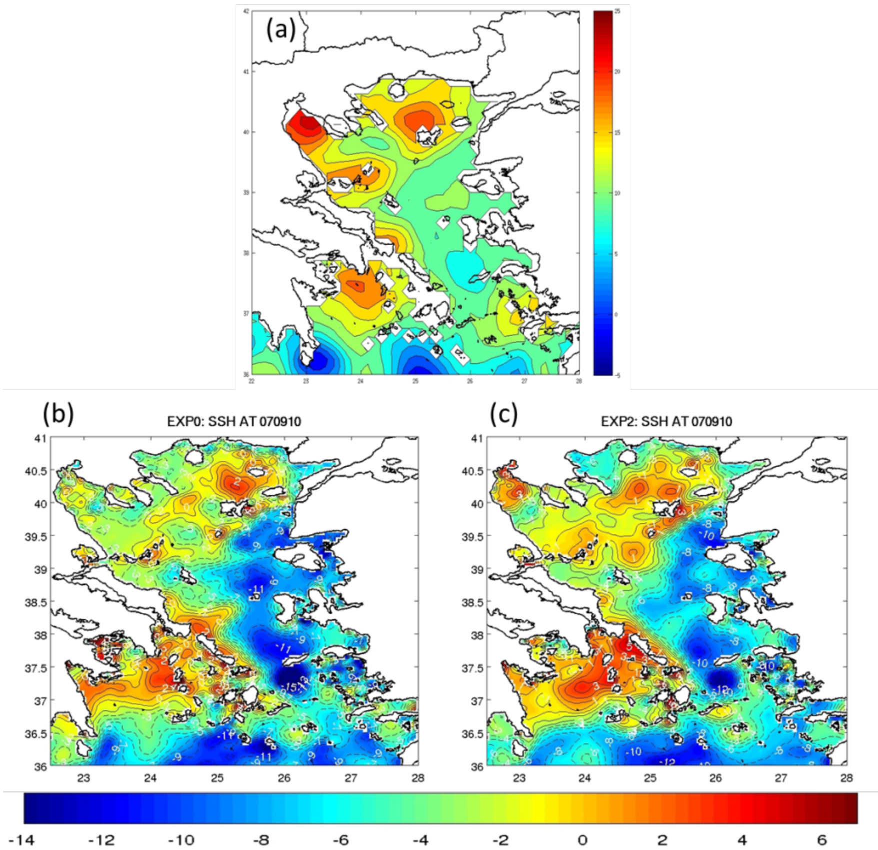

Figure 3.7: Sea surface height at 07.09.10 corresponding to a) Satellite altimetry b) the analysis of EXP0 c) the analysis of EXP2.

3.2.2 The assimilation of FerryBox SST data into the Aegean Sea model.

Two assimilation experiments were performed over the period mid-August 2012 – mid-January 2013 in order to evaluate the performance of the assimilation system and estimate the impact of Ferrybox SST data assimilation process in the model along the route from Piraeus to Heraklion as explained in Table 3.2. In the first experiment (control run - CTRL) the Aegean Sea model is integrated for the 6-month period nested with the MFS model and assimilating satellite SSH, SST data and Argo T/S profiles on a weekly basis using the localized SEEK filter. In the control run of the model the Ferrybox data were retained for the assimilation process in order to be used as independent observations for the assessment of the daily system performance. In the second experiment (EXP1) the system additionally to the previous sets of data is assimilating SST observations over the route from Pireaus to Heraklion on a daily basis. For the whole 5-month period, the Ferrybox data are assimilated every day at 00:00 UTC. The interval 24.10.12 – 05.12.12 Ferrybox data were not available due to regular system maintenance. SSS Ferrybox data also acquired by the FerryBox system were excluded from the assimilation process due to a systematic drift of the conductivity sensor that could not be corrected at an acceptable for assimilation system manner.

Table 3.2: Description of the different experiments performed with the Aegean Sea model over the period 05.04.10 – 31.12.10

Experiment	Period of model integration	Observations	Frequency of data assimilation
CTRL	14.08.12 – 15.01.13	Satellite SSH-SST and T/S ARGO profiles	Weekly
EXP1	14.08.12 – 15.01.13	Satellite SSH-SST, T/S ARGO profiles, SST observations along the FerryBox route	Daily for SST FeeryBox data. The rest of observations are assimilated on a weekly basis

The weekly assimilation of satellite SSH and SST data into the modelling system for the 5-month period mid-August 2012 – mid-January 2013, showed the ability of the filter to fit the assimilated data within the specified uncertainties. The additional assimilation of daily FB SST data, re-confirmed previous findings of the local importance of FB data assimilation data within the south Aegean Sea (Korres et al., 2009) and showed their significant role in setting certain dynamical features within this area. It was demonstrated that the daily data assimilation of these data significantly improves the performance of the model with respect to both SST, SSH and the subsurface circulation fields. More specifically, the correct representation in the model solution of the existing dipole (cyclone – anticyclone) or tripole within the southern Aegean Sea can be crucially dependent upon the introduction of observations along ferry tracks. In these 5-months test period, we have shown at least one case where the sea surface height distribution over the southern Aegean Sea and the subsurface flow field have changed significantly after the assimilation of FB SST data.

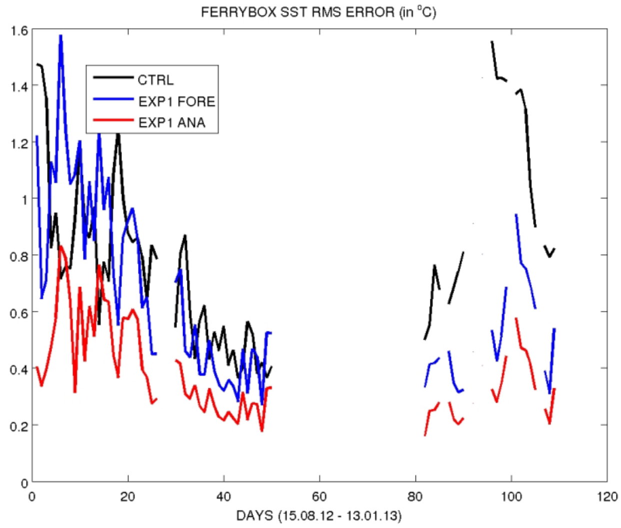

Figure 3.8: Forecast and analysis SST RMS error for the CTRL and EXP1 experiments.

The forecast and analysis RMS errors for SST and SSH with respect to observations (daily FB SST data and weekly satellite gridded SSH maps) are shown in fig. 3.8 and fig. 3.9a,b for CTRL & EXP1 experiments. The forecast RMS error is computed just before the analysis update and can be considered as an indicator of the consistency between the model dynamics and the filter statistics. The SST forecast RMS error (fig. 3.8) after the first 15 days of assimilation, becomes lower than the forecast error of the control run. This initial period of 15 days can be considered as the time period necessary for the system to adjust to the new data brought in by the data assimilation. On the other hand the analysis SST RMS error of EXP1 is always lower than the forecast error of CTRL experiment. The fact that the SST forecast error of EXP1 is always lower than the free run error and at a small distance to the analysis error indicates that the statistical correction introduced by the assimilation scheme is consistent with the model's dynamics. It is very important to note that the daily assimilation of SST FB data along the ferry track as it is done in EXP1 is able to further reduce the analysis (fig. 3.9a) and forecast (fig. 3.9b) SSH RMS errors with respect to the control experiment implying statistically significant cross-correlations between the two variables. Considering that the circulation of the Cretan Sea is mainly dictated by a dynamic dipole consisting of mesoscale cyclonic and anticyclonic eddies with pronounced signature on the observed SST and SSH (Cardin et al., 2003), it is reasonable to expect that the additional assimilation of FB SST data along tracks that partially cross the dipole will have a measurable effect on the analysis of the sea surface relief of the area. It is worth noting that such a positive impact is not occurring in other observed model variables as for example the salinity profiles from ARGO floats, which for the time period of our experiment are outside the South Aegean Sea.

The results of this study have been recently published in Korres et al. (2014).

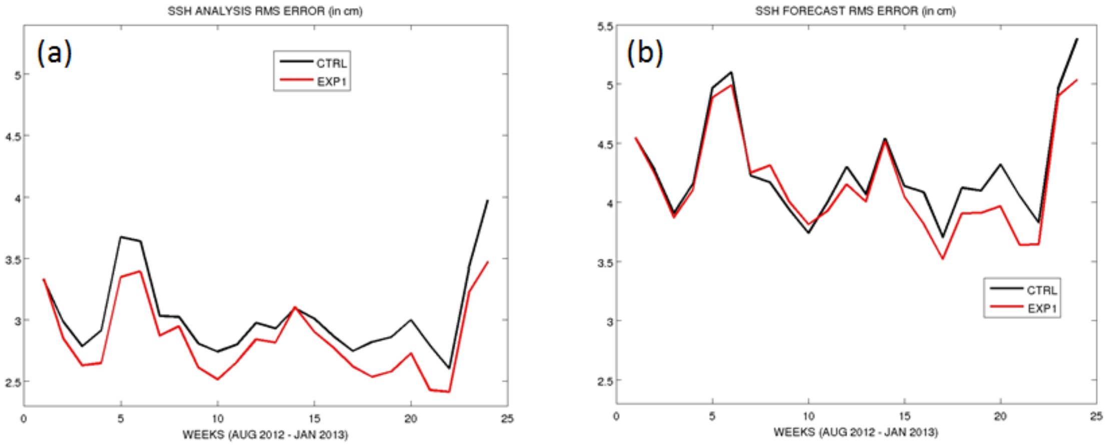

Figure 3.9: a) SSH analysis RMS error (in cm) corresponding to the experiments CTRL and EXP1 b) SSH forecast RMS error (in cm) corresponding to experiments CTRL and EXP1.

4. OSE in the German Bight - North Sea (HZG)

4.1 OSE Experiments setup

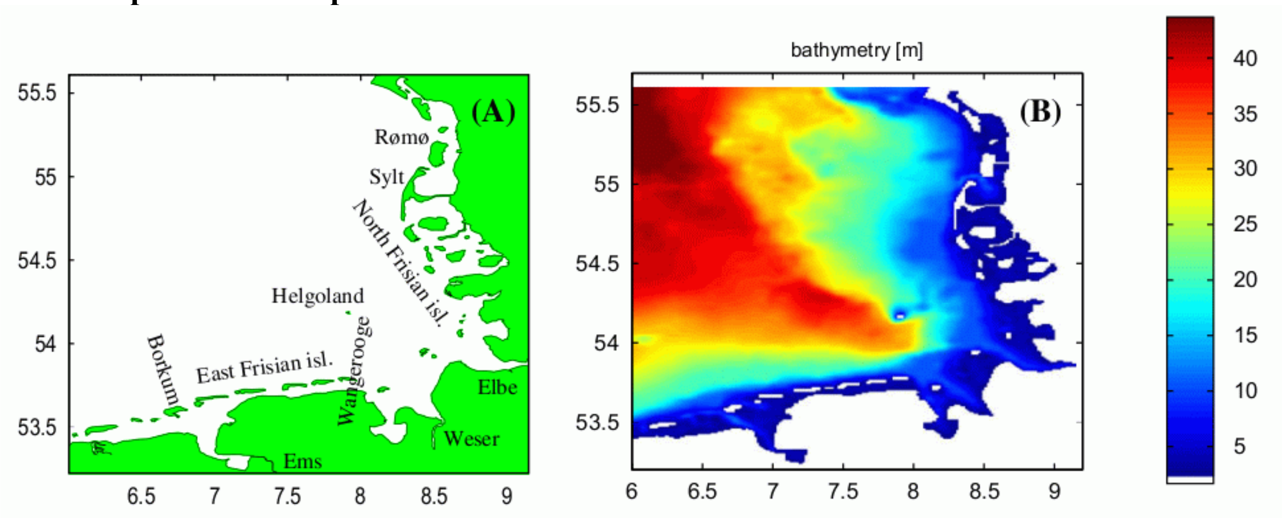

Fig. 4.1: A) Map of the German Bight B) Bathymetry of the German Bight

4.1.1 Geographical setup

The German Bight is the southeastern bight of the North Sea bounded by the Netherlands and Germany to the south, and Denmark and Germany to the east. To the north and west it is limited by the Dogger Bank. The Bight contains the Frisian and Danish Islands. The German Bight is dominated by tides with a typical tidal range of 2–4 m and a dominant period of 12.4 h. The largest non-tidal variations are caused by atmospheric low pressure systems, either as external surges from the North Atlantic or internally generated surges. During strong storm events water levels can exceed 4 m above mean sea level. The German Bight is furthermore characterised by very shallow water with Wadden Sea areas falling dry during low tide. The region is very busy regarding offshore operations (e.g. offshore wind farms) and ship traffic (e.g., to the harbor of Hamburg). Apart from the complicated tidal dynamics as e.g. described in Stanev et al. (2014), sediment transport and current/ocean wave interaction processes play an important role.

4.1.2 Model Description

In this study, the 3-D numerical model GETM (Burchard and Bolding, 2002) is used to simulate the hydrodynamical processes in the German Bight. A map of the German Bight and the bathymetry of the 203 km by 258 km model domain is shown in Fig. 4.1 (A) and (B), respectively. GETM is a primitive equation model, in which the equations for the three velocity components and sea surface height, as well as the equations for turbulent kinetic energy and the eddy dissipation rate are solved. The application of the model to the area of our study is described in Staneva et al. (2009). The model is run on a spherical grid with 1 km resolution. Terrain following equidistant coordinates (sigma-coordinates) is used for the vertical dimension. The water column is discretised into 21 non-intersecting layers. The model system is forced by: (1) the meteorological forcing derived from bulk formulae using wind, mean sea level pressure, air temperature, humidity

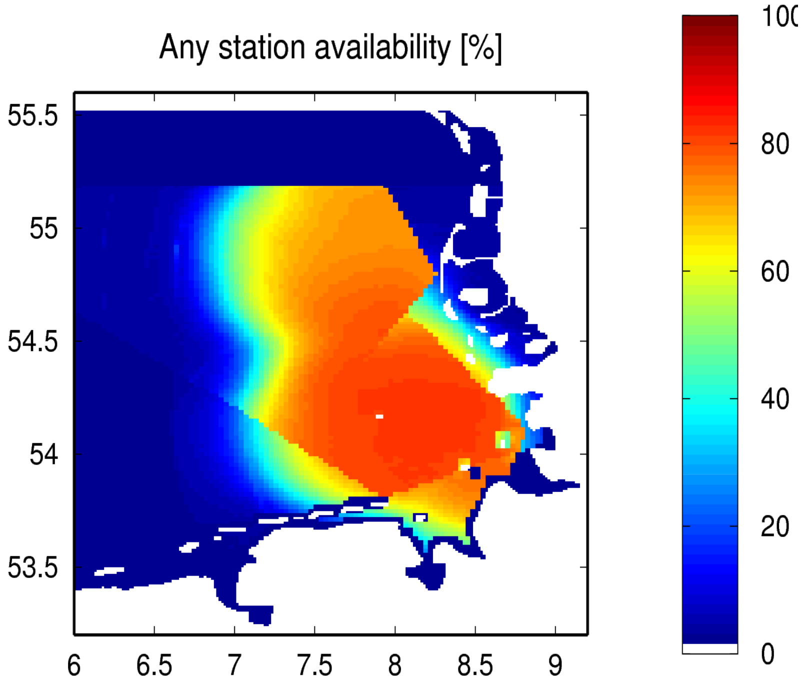

Fig.4.2 : Availability of at least one radial component from one of the three existing HF radar stations located at Wangerooge,

and cloud cover taken from the hourly forecasts of the German Weather Service (DWD) COSMO-EU model with 7 km horizontal resolution, (2) river inflows from climatological data for the 30 most important rivers within the North Sea-Baltic Sea model area provided by the Swedish Meteorological and Hydographical

Institute (SMHI) and BSH river-runoff data for the German Bight model setup, (3) time varying lateral boundary conditions for sea surface elevation, temperature and salinity. Temperature and salinity of the western and northern open boundaries of the German Bight are taken from the North Sea-Baltic Sea model output; the North Sea and Baltic Sea with coarser resolution (about 5 km) uses the same computational code (GETM). The method proposed by Flather (1976) is used for the barotropic variables. The tidal forcing at the open boundaries of the North Sea-Baltic Sea model towards the Norwegian Sea and the English Channel was constructed using 13 partial tidal constituents obtained from satellite altimeter data via the OSU Tidal Inversion Software Egbert and Erofeeva (2002). Temperature and salinity at the open boundary are interpolated from monthly mean climatological data described in Janssen et al. (1999). The model is initialized with data from the operational COSYNA model (http://www.cosyna.de).

4.1.3 Data assimilation system description

The analysis scheme applied for HF radar data is basically a spatio/temporal optimal interpolation technique. The method uses analysis windows of 13 hr length for hindcast computations and of 24 hr length for short term forecasts. The analysis includes the tidal time scale. For forecasts the analysis window is split into a hindcast and a forecast interval. Details about this technique are given in Stanev et al. (2014). The window size is chosen such that at least one tidal cycle is contained in the hindcast interval of the analysis period. Using this approach a continuous surface current trajectory over one or two M2 tidal cycles is obtained. This is in contrast to the traditional filter approach where an analysis with a corresponding trajectory jump is performed, whenever observations are available.
In a classical filter method such discontinuities usually occur at the time of the analysis and model restart, because the analysis does not take into account correlations of the model state in time. The proposed block-wise analysis has particular advantages for HF-radar data where measurements are taken at short intervals like 20 minutes for the radar system used in this study. To increase the area with available measurements and to avoid any issues related to the processing of two dimensional current vectors from HF-radar data, radial components are used as input for the analysis instead of zonal and meridional components.

4.1.4 Observational Data Sets

An ocean surface current transporting the Bragg resonant ocean waves causes a Doppler shift (Barrick,1978; Stewart and Joy, 1974). This shift can be converted to the underlying current speed towards or away from the radar, which is the radial component ur of the 2-dimensional (2D) surface current. Based on this principle, three HF radars have been installed on the island of Wangerooge, at Büsum, and on the island of Sylt to monitor ocean currents and waves in the German Bight. These systems cover the eastern part of the German Bight and are WERA type radars (Gurgel et al., 1999) operated in the 10.8 MHz (Büsum and Sylt) and 12.1 MHz (Wangerooge) frequency range. The spatial resolution is 1.5 km in range and about 3 degrees in azimuth. Measurements are taken every 20 min and represent 10 min averages. Due to the working frequency, the radar couples to 12.5 m (12.1 MHz) and 13.9 m (10.8 MHz) long ocean waves by Bragg scattering and the radar echoes provide information on ocean currents within a surface layer of about 1 m (Stewart and Joy, 1974). The working range of the WERAs mainly depends on salinity, sea state, working frequency, and electromagnetic noise (Radio Frequency Interference (RFI), background noise, and ionospheric reflections). Typically the radar reaches out to 120 km off the coast. The range and coverage achieved by the antenna stations is illustrated in Fig.4.2. Colors indicate the percentage of available measurements for the three stations.

4.2 Discussion of results

The analysis method was applied to three month of data acquired in 2011. Two analysis examples are shown in Fig. 4.3 for March 22, 11:00 UTC (top left) and 17:00 UTC (top right). The free run is in blue, the HF radar data in green and the analysis in red. It was demonstrated that the method is able to improve the agreement with the HF radar observation data on a statistical basis. Figure 4.3 (bottom) shows the respective innovations (difference between free run and observations) and the residual (difference between the analysis and the observations) for the radial current component of the Büsum station. One can see that the rms values are in fact smaller for the residual than for the innovation for the most part. Only in the very shallow water regions close to the coast where both the numerical model and the HF radar are expected to have bigger errors the reduction is not as strong.

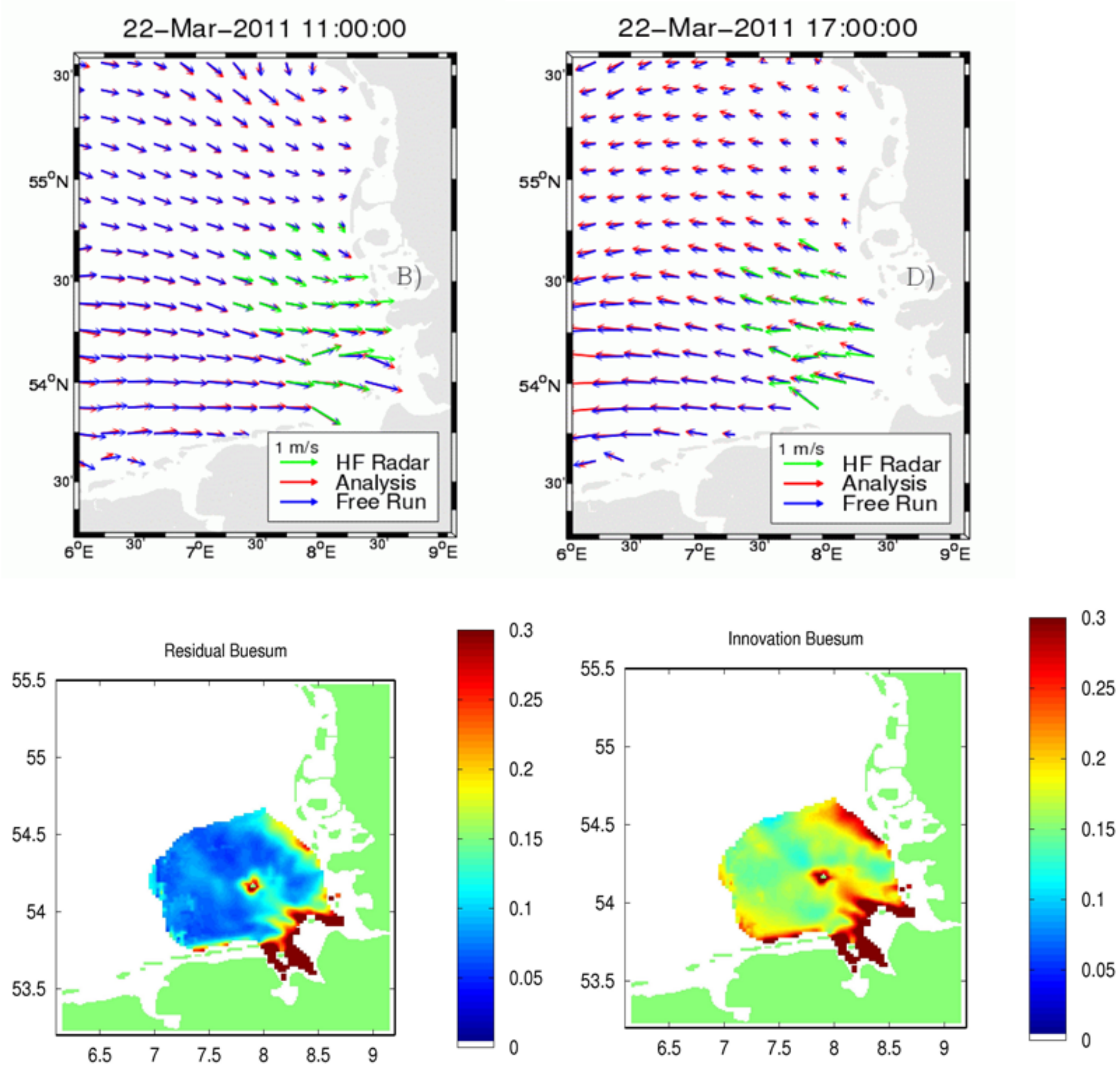

Fig.4.3: (top) Analysis examples with free run in blue, HF radar data in green and analysis in red for March 22, 2011 11:00 UTC (top left) and 17:00 UTC (top right). (bottom) Innovation (bottom left) and residual (bottom right) for the Büsum radial current component.

Comparisons with independent ADCP measurements taken at the FINO-1 and FINO-3 platform confirmed that the analysis is in fact able to improve the free run. The FINO-3 platform is only covered by the Sylt antenna station, i.e., there is no directional current information from the radar available at that location. The FINO-1 station is not covered by any of the HF radar stations. The fact that a small improvement was also found for this location demonstrates the upscaling capability of the analysis approach. One analysis example is given in Fig 4.4 (left).

It was furthermore shown that the HF radar data are able to improve the surface current forecast over a period of up to 12 hours. Fig 4.4 (right) shows the analysis skill (red curve) in comparison to the persistence skill (blue curve) for the zonal current component. These curves represent spatial averages over the area where both current components are available from the HF radar. The skills within the analysis window of 24 hours were obtained by averaging over the entire considered period of three month. As one can see the analysis does show a positive skill for the entire forecast period and is always better than the persistence. Further details are given in (Stanev et al, 2014)

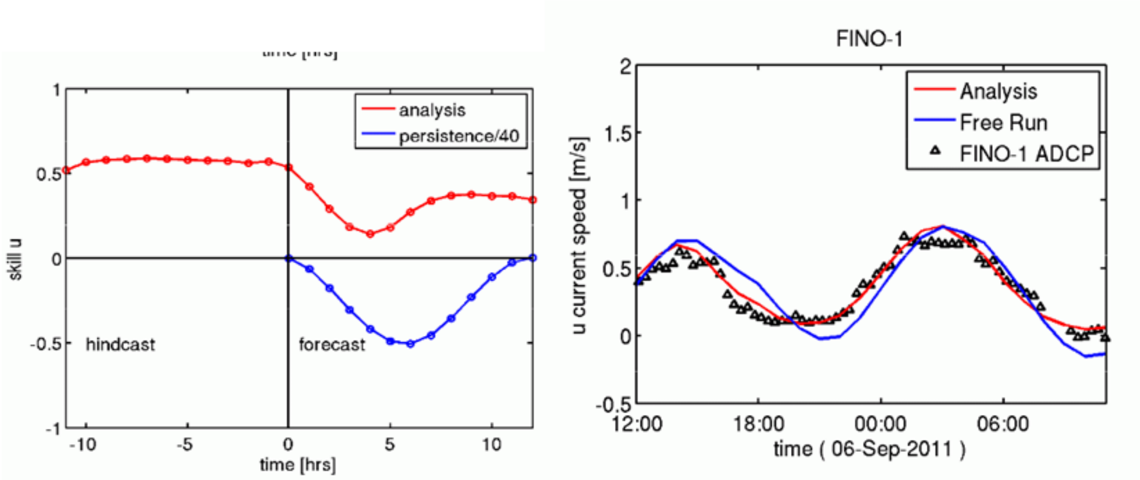

Figure 4.4: (Left) Comparison of the surface current analysis (red) with the free run (blue) and the ADCP data taken at the FINO-1 platform (black triangles). (Right) Comparison of the analysis skill with the persistence skill within the analysis window of 24 hours including 12 hrs hindcast and 12 hrs forecast

5. OSE in the North Sea (DELTARES)

5.1. Setup of experiments

5.1.1 Geographical set-up

The North Sea is located between Great Britain, Belgium, the Netherlands, Germany, and Scandinavia. It connects to the Atlantic Ocean through the English Channel in the south and the Norwegian Sea in the north. In the east, it connects to the Baltic Sea. The main pattern of water flow in the North Sea is anti-clockwise rotation along the edges. It receives the majority of ocean current from the northwest opening and a smaller portion from the opening at the English Channel (Figure 5.1).

Figure 5.1. Amphidromic system of the M2 constituent in the North Sea (taken from http://en.wikipedia.org/wiki/Amphidromic_point)

5.1.2 Model description

Since recently, the Dutch Continental Shelf Model version 6 (Figure 5.2) has been used operationally for water level forecasts in the North Sea (Zijl et al. 2013). This model will replace the previous operational system that is based on a sequence of models (DSMv5, ZUNOv4, Kuststrook Fijnv6) (Verlaan et al. 2005).

DCSMv6 has been developed as an application of SIMONA, a framework for hydrodynamic modelling of free-surface water systems. Within the SIMONA framework, the WAQUA module is used for modelling 2D (horizontal) schematizations of water systems. DCSMv6 uses spherical grid that has a uniform cell size of 1.5’ (1/40°) in east-west direction and 1.0’ (1/60°) in north-south direction. This corresponds to a grid cell size of about 2 by 2 km. The grid is specified in geographical coordinates and covers the area between 15° W to 13° E and 43° N to 64° N (Figure 5.2). The model area of DCSMv6 has been extended in order to ensure that the open boundary conditions are located further away in deep water. This makes it possible to use harmonic boundary forcing derived from global tidal models. Furthermore, wind setup in deep water can safely be neglected, whereas the effect of local pressure (the so-called inverse barometer effect) is added to the water level variation along the open boundary.

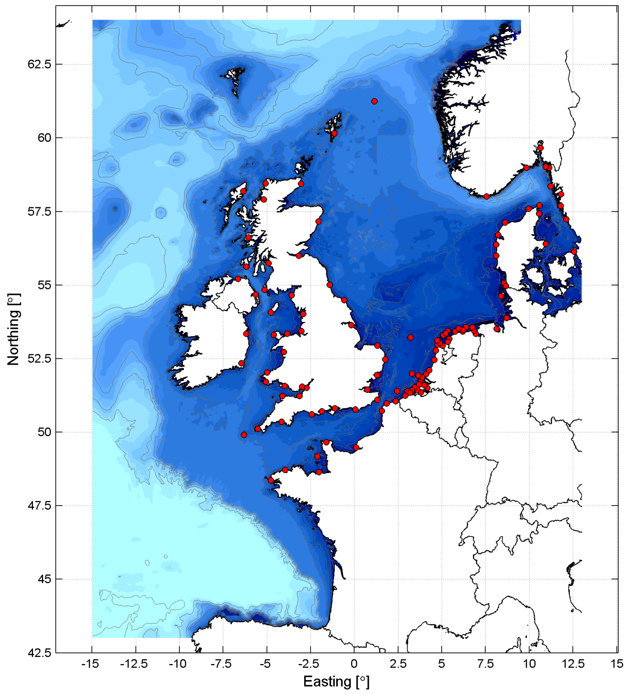

Figure 5.2: DCSMv6 area and overview of tide gauge stations available for calibration and validation.

The model bathymetry is specified on the cell corners of the DCSMv6 model grid. Depths at the location of the cell centres (where water levels are specified and computed) are determined by using the mean value of the surrounding values at the cell corners. The DCSMv6 area covers an area where bathymetry varies from more than 2000 meter in the northern part down to less than 50 meter in the southern North Sea.

At the northern, western and southern sides of the model domain, open water level boundaries are defined. Water levels are specified at 205 different locations along those boundaries. In between these locations the imposed water levels are interpolated linearly. The imposed water levels at the open boundaries can be splitted in tidal and non-tidal components. The tidal water levels at the open boundaries are specified in terms of amplitudes and phases of a number of tidal constituents are specified. The tidal conditions of the eight main diurnal and semi-diurnal constituents have been derived by interpolation from a dataset derived from the GOT00.2 global tidal model. These eight tidal constituents (in order of increasing angular velocity) are Q1, O1, P1, K1, N2, M2, S2 and K2. Some smaller diurnal and semi-diurnal constituents have been added later. These smaller constituents have been derived from the eight main constituents by means of the admittance method. The smaller constituents added are MU2, NU2, LABDA2, T2, 2Q1, SIGMA1, RO1, M1, CHI, PI1, FI1, THETA1, J1, OO1, 2N2 and L2. In addition, the annual constituent Sa is also used; this has been determined from satellite altimetry data. While wind setup at the open boundary is neglected because of the deep water there, the (non-tidal) effect of local pressure can be significant. This so-called inverse barometer effect varies in time and space (dependent on the local atmospheric pressure) and is added to the tidal water level variation along the open boundary.

Tide Generating Forces (TGF), recently implemented in SIMONA, have been switched on in the DCSMv6 model. The effect of TGF has an amplitude in the order of 10 cm throughout the model domain (determined with a preliminary version of the model). Components of the tide with a Doodson number from 55.565 to 375.575 have been included. Consequently, the constituents M0 and S0, which would have caused a static elevation that varies in space, are excluded.

For meteorological forcing of the DCSMv6 model use has been made of time- and space varying wind (at 10 m height) and pressure (at MSL), derived from HIRLAM. For the calibration and validation of DCSMv6 hindcast data from HIRLAM version v7.0 is used, with output available every 3 hours. For interpolating the wind and pressure fields on the DCSMv6 grid, the HIRLAM land-sea mask has been taken into account. Cells that are more than 50 % land are excluded from the HIRLAM wind and pressure fields and where necessary extrapolated based on the data at surrounding points.

5.1.3 Data assimilation scheme

Like in the previous operational system, a data assimilation procedure based on a steady state Kalman filter is implemented with the DCSMv6 model. The steady state Kalman filter assimilates 10-minutely in situ observed water level data into the DCSMv6, with a hindcast-forecast cycle of six hours (Heemink and Kloosterhuis, 1990).

In the Kalman filter, it is assumed that the source of uncertainty is due to the wind input. An autoregressive model AR(1) is used to represent this error process. Further, the covariance of this error is assumed to be isotropic in space and constant in time. As for the observational error, a Gaussian white noise with standard deviation of five centimeter is assumed for each observation.

The steady state Kalman gain is determined by using an ensemble Kalman filter. First, an ensemble Kalman filter with the above-mentioned error specifications is used with the DCSMv6 off-line, to generate a series of Kalman gains at various time levels. The steady state Kalman gain is obtained by simply averaging these Kalman gains over time. The generic data assimilation software OpenDA (Verlaan, et al., 2010) is used both for the preparation of the Kalman gain as well as for the operational steady state Kalman filter.

In building the Kalman filter, a question that should be answered was which stations should be used for data assimilation? The Observing System Experiments (OSE) could be used to answer this question. In this study, however, we have used an approximate method of OSE for estimating observation impact. The method is originally proposed by Langland and Baker (2004) for estimating impact of various observations in the framework of variational data assimilation. The method avoids the data withdrawal experiments of the OSEs and estimates observation impact by using only one model run. Liu and Kalnay (2008) proposed a variant of this method in the framework of ensemble Kalman filtering. In this study, we extended this method further to a steady state Kalman filtering framework (Sumihar and Verlaan, 2010). This last method was used in this study to gain insight about observation impact on the accuracy improvement of the forecasts generated by the DCSMv6.

The method estimates the impact of data assimilation on forecast accuracy, where the measure of forecast accuracy is defined as a quadratic cost function of observation-minus-model residuals. It uses simply timeseries of observation and the corresponding model output generated without data assimilation. Therefore, it is applicable even before a Kalman filter is actually implemented.

5.1.4 Observational data sets

A large number of tide gauges are available for the calibration and validation of DCSMv6 (Figure 5.2). Observed water level is available with a time step of 10 minutes. The observations are available via the NOOS exchange (www.noos.cc).

5.2. Results and discussions

Some results of the observation impact analysis for the DCSMv6 are shown in Figure 5.3 and Figure 5.4. In this case, the cost function is computed over 13 stations along the Dutch coasts and over the whole year 2007. Note that ΔJ is defined as cost of with data assimilation minus cost of without data assimilation. A negative value means, therefore, accuracy improvement.

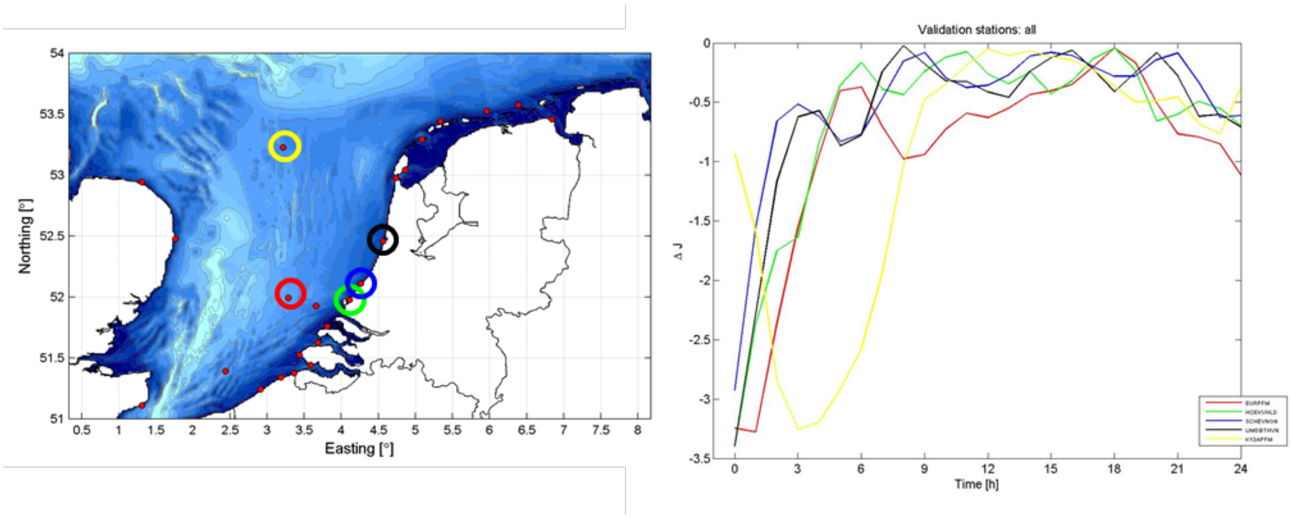

Figure 5.3: Selected observing stations nearby the Dutch coasts (red dots; left panel) and averaged impact of five stations (right panel; color of each line corresponds to the color of the circle surrounding each station on the left panel)

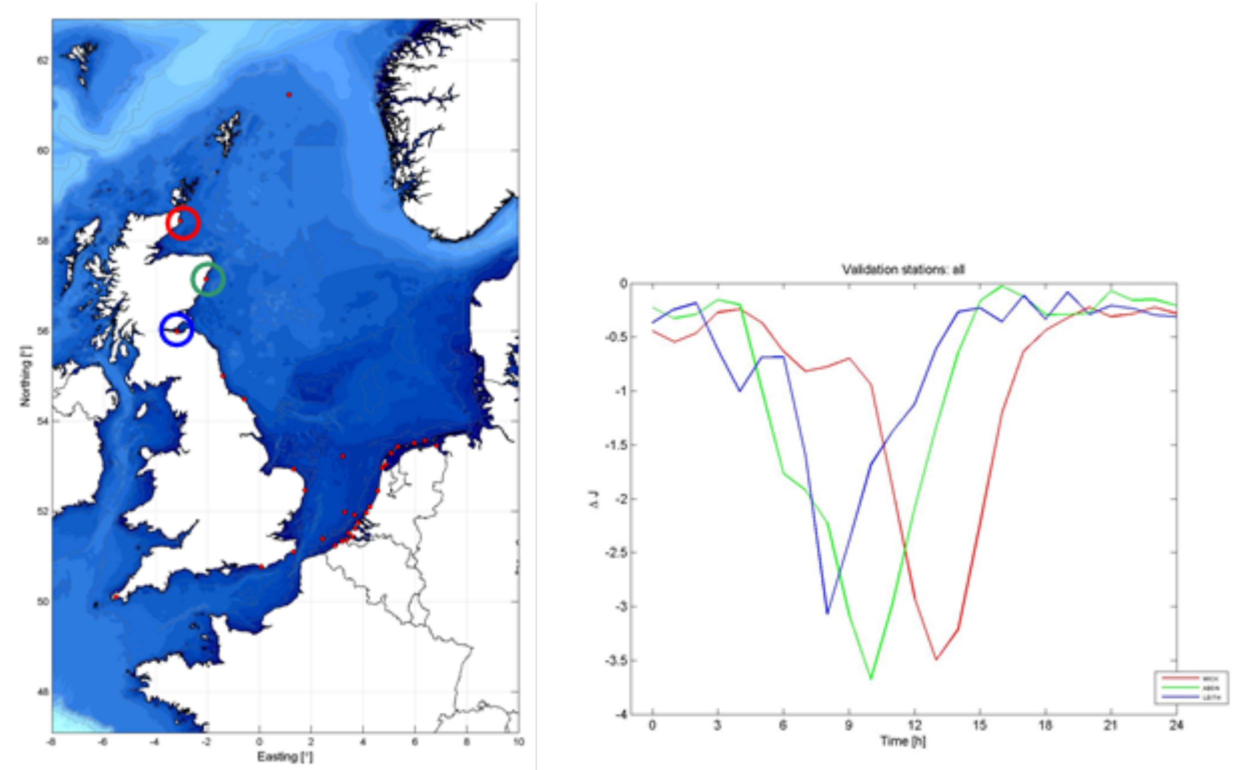

Figure 5.4: All 32 selected observing stations (red dots; left panel) and averaged impact of three stations on the northern British coasts (right panel; color of each line corresponds to the color of the circle surrounding each station on the left panel).

As can be seen from these figures, assimilating water level data from the indicated stations is expected to improve the model accuracy. Assimilation stations located nearby the validation stations have immediate impact on the accuracy improvement. After sometime, the impact vanishes. On the other hand, the impact of stations located further away upstream of the validation stations comes later. The time before the maximum impact of an assimilation station arrives is related to the gravity wave propagation from the assimilation station to the validation stations.

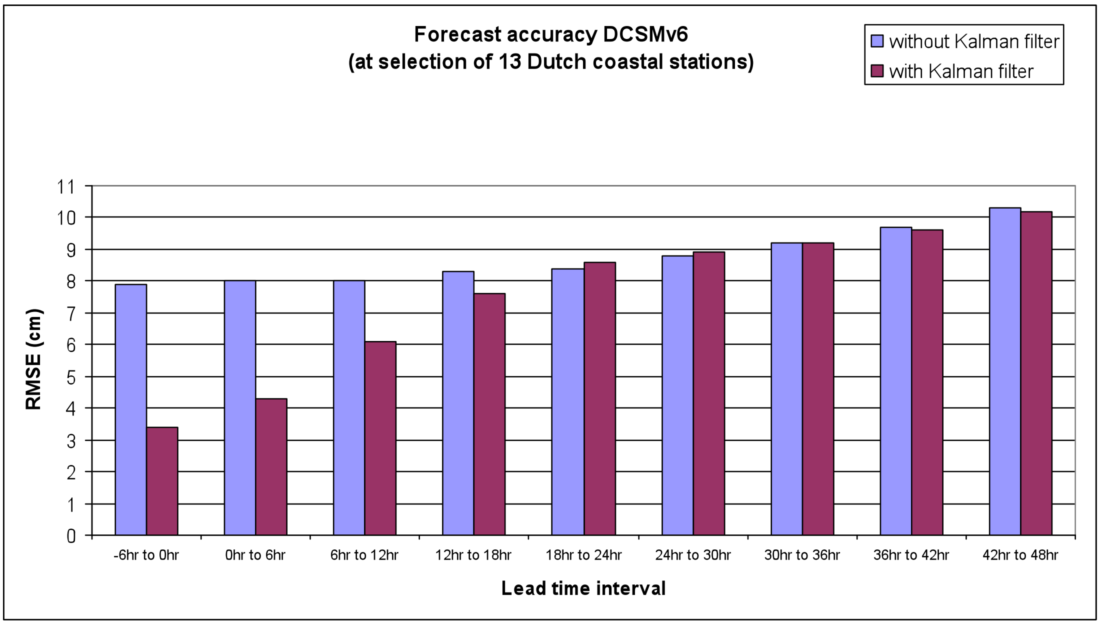

Figure 5.5: Performance of DCSMv6 without and with Kalman filter, in term of root mean square of water level residuals averaged over 13 stations along the Dutch coasts.

Using this method, 32 stations have been selected for data assimilation (Figure 5.4). The forecast performance of the DCSMv6 with and without data assimilation is shown in Figure 5.5, in term of forecast RMSE, computed over the same 13 validation stations mentioned earlier. The figure shows that the impact of data assimilation is significant in the short lead time forecast. The impact decreases gradually and the performance converges to the deterministic underlying model after 18 hours.

6. OSE in the North Sea (MUMM)

6.1. OSE experiment setup

6.1.1 Geographical area

The North Sea domain under consideration is located between 4°W to 10°E in longitude and 48.5°N to 60°N in latitude. There are three open sea boundaries: a narrow connection to the English Channel through the Dover Strait, a connection to the Baltic Sea through the Skagerrak, and a wide northern boundary. Its bathymetry varies widely, with large areas that are less than 40 metres deep (Southern and German Bights as well as the Dogger Bank) while there are deeper regions east and west of the Dogger Bank where the depths exceed 90 meters. Along the Norwegian Trench, the depth is up to 700 meters. The most important forcing mechanisms are the tides and the wind. Semi-diurnal tides are predominant at the latitude under consideration. The dominant factor governing the temperature field is the surface seasonal heating and cooling which, in the central part of the North Sea, leads to a thermal stratification of the water column in summer.

6.1.2 Model description

The COHERENS (Coupled Hydrodynamical-Ecological Model for Regional and Shelf Seas) model (Luyten, 2011) is a finite difference model. Simulations are performed with a horizontal resolution of 4 nautical miles in the horizontal, 20 σ-sigma levels in the vertical and a time step of 20 seconds.

Meteorological data are supplied by the Danish Meteorological Institute (DMI) from the HIRLAM model with a temporal resolution of one hour. Tidal harmonics and daily profiles of currents, temperature, salinity and inflow/outflow conditions at the boundaries of the domain are derived from simulations with the POLCOMS (Proudman Oceanographic Laboratory) model covering a larger area. River runoffs from the Elbe, Scheldt, Rhine/Meuse, Thames, Humber, Tyne/Tees are taken into account. Baroclinic inflow/outflow conditions are imposed at the eastern boundary to include the exchange of water masses with the Baltic Sea.

6.1.3 Data assimilation system description

The ensemble Kalman filter developed by Evensen (1994) combines the traditional Kalman filter with Monte-Carlo methods to generate an ensemble of states representing the model error. Two square root algorithms is applied at the analysis step: the square root algorithm in which data are considered as perfect and a low rank square root algorithm allowing an ensemble representation of the observations error.

Simulations are carried out for September 2001, a month during which the two dynamical regimes of the North Sea coexist (well mixed and summer stratified). An initial ensemble of states is generated from the 1st of September and is integrated without data assimilation till the 11th of September. The model error is sampled once a day using 50 ensemble members. Eight temperature profiles are assimilated once a day at midnight from the 12th of September till the 28th of September.

Synthetic temperature profiles are assimilated, they are derived using the above mentioned model setup with a horizontal resolution of one nautical mile. They show significant differences in comparison with the temperature modelled with a horizontal resolution of four nautical miles [She et al., 2006]:

- eddy structures with scales of a few kilometers, visible along the thermal fronts in the one nautical mile resolution simulations, not resolved by the coarser grid,
- large vertical displacements of the thermocline: this feature of the North Sea dynamics is induced by winds and tides, the amplitudes are much larger in the high resolution run.

6.1.4 Data sets

It has been chosen to focus on a network of buoy data for two reasons. First, satellites provide surface data with a very high spatial coverage and a temporal resolution of around one day. However, even in cloud free conditions their errors remain larger than that from CTD in situ data. Furthermore, no vertical information is available from satellite data while profile measurements can be provided either by CTD data or buoys. CTD or buoy data have a very high temporal resolution but are limited to a fixed location and exist only at a few locations; such data can be transferred in near real time and are less expensive to operate than satellites.

The data set consists of 20 temperature profiles. They are extracted at the assimilation time step from model runs generated with the same set-up but with a higher horizontal resolution of one nautical mile. Their impact on the neighboring temperature field is limited by means of an assimilation cutoff radius. Eight stations were selected amongst the existing network of stations in the North Sea.

The existing North Sea network of observations examined at this stage is made of eight buoys extracted at existing observation locations (Figure 6.1). They are located along the Belgian coast, in the German Bight and in the United Kingdom central part of the North Sea. Such locations take into account the two dynamical regimes of the North Sea in summer. Two stations are highlighted in red (station 10 and station 19) representing respectively a well mixed and a stratified regime.

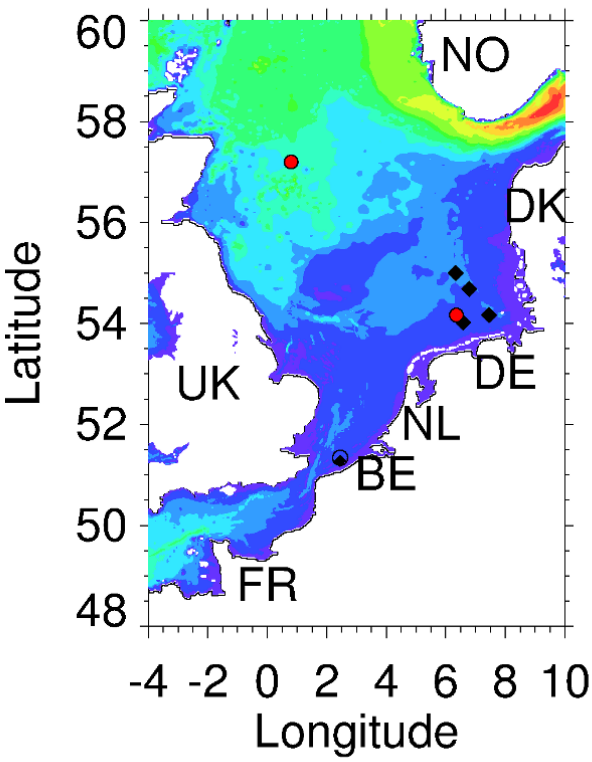

Figure 6.1: Stations of the North Sea existing network where temperature profiles are assimilated.

6.2. Discussion of some results

Sea surface temperature

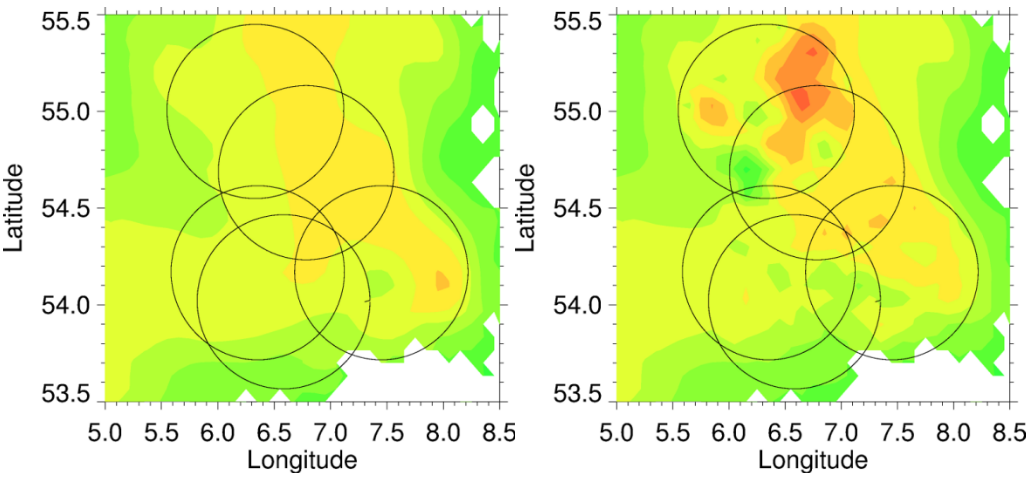

Figure 6.2: Modelled sea surface temperature in the German Bight on the 28th of September 2001, without (left) and with (right) data assimilation

Figure 6.2 provides a zoom on the surface temperature of the German Bight on the last day of the assimilation period (the 28th of September 2001). The left panel represents the temperature without data assimilation while the right panel corresponds to the temperature with data assimilation. The circles have a radius of 50km and are centered on the stations at which data are assimilated.

The impact of the assimilation radius is clear and the assimilation process provides a warmer surface temperature in most cases.

Temperature profiles

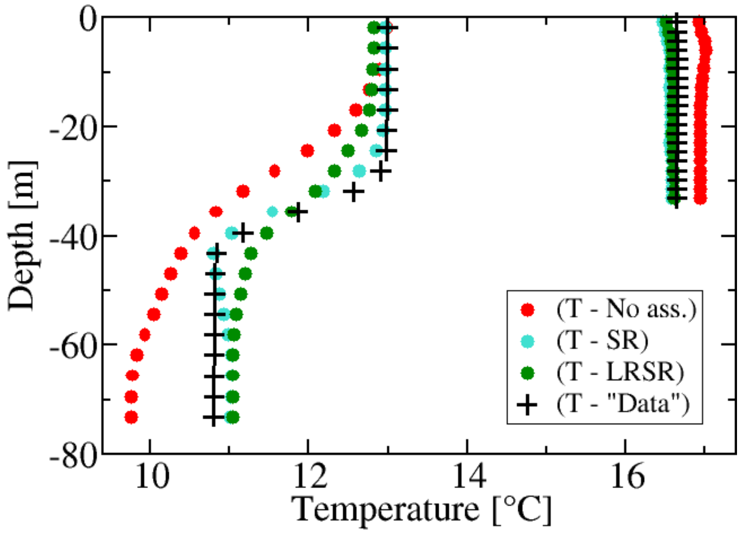

Figure 6.3: Impact of the assimilation of temperature profiles at two stations (10 and 19)

Figure 6.3 represents modelled temperature profiles at station 10 (well mixed) and at station 19 (stratified). The red dots correspond to the temperature modelled without data assimilation, the dark green dots to the temperature modelled with the low rank square root algorithm, the light blue dots to the temperature modelled with the square root algorithm. Black crosses correspond to the assimilated data.

At well mixed station 10, the temperature modelled with data assimilation is very close to the assimilated data. The assimilated data are colder than the model without data assimilation. Results from the low rank square root algorithm are very slightly closer to the assimilated data than those obtained with the square root algorithm. A possible explanation to this feature is the influence of assimilated data at neighboring stations in the German Bight.

Temperature profiles at stratified station 19 show that the largest differences between the non assimilative model and the assimilated data take place at the bottom. Results obtained with the square root algorithm reproduce sharply the position of the thermocline in the assimilated data. The agreement with the assimilated data at 50 metres depth is particularly good. Below that depth, they are diverging from the assimilated data. This is attributed to the fact that the corrections applied to the temperature are too strong and perturb the model dynamics which, in turn, influences the temperature at that station.

The above results indicate a large range of discrepancies between model and data depending on the dynamical regime of the North Sea area under study. When the ensemble is generated to represent adequately that range of model error, the ensemble Kalman filter allows to improve the modelled temperature to a very high degree of agreement with the data.

References

Adcroft, A., Hill, C., & Marshall, J. (1997). Representation of topography by shaved cells in a height coordinate ocean model. *Monthly Weather Review, 125(9),* 2293-2315.

Barrick, D.E. "HF Radio Oceanography - a Review." *Boundary Layer Metereology* 13 (1978): 23-43.

Burchard, H., and K. Bolding. *GETM - a General Estuarine Transport Model*. European Comission, 2002.

Cardin, V., M. Gacic , K. Nittis, V. Kova and L. Perini, 2003: Sub-inertial variability in the Cretan Sea from the M3A buoy. Annales Geophysicae, 21, 89-102.

Dobricic, S., Pinardi, N., Adani, M., Tonani, M., Fratianni, C., Bonazzi, A., & Fernandez, V. (2007). Daily oceanographic analyses by Mediterranean Forecasting System at the basin scale. *Ocean Science, 3(1),* 149-157.

Dobricic, S., & Pinardi, N. (2008). An oceanographic three-dimensional variational data assimilation scheme. *Ocean Modelling, 22(3),* 89-105.

Egbert, G., and S. Erofeeva. "Efficient Inverse Modeling of Barotropic Ocean Tides." *Journal of Atmospheric and Oceanic Technology* 19 (2002): 183–204.

Evensen, G., 1994. Sequential data assimilation with a nonlinear quasi-geostrophic model using Monte Carlo methods to forecast error statistics, Journal of Geophysical Research, 99, 10 143- 10 162, 1994.

Falco, P., Belardinelli, A., Santojanni, A., Cingolani, N., Russo, A., & Arneri, E. (2007). An observing system for the collection of fishery and oceanographic data. *Ocean Science, 3(2),* 189-203.

Flather, RA. "A Tidal Model of the North-West European Continental Shelf." *Mem Soc R Sci Liège, Ser 6* 10 (1976): 141–64.

Gunduz, M., Dobricic, S., Oddo, P., Pinardi, N., & Guarnieri, A. (2013). Impact of Levantine Intermediate Water on the interannual variability of the Adriatic Sea based on simulations with a fine resolution ocean model. *Ocean Modelling, 72,* 253-263.

Gurgel, K.-W., G. Antonischki, H.-H. Essen, and T. Schlick. "Wellen Radar (WERA): A New Ground Wave HF Radar for Ocean Remote Sensing." *Coastal Engineering* 37 (1999): 219–134.

Heemink, A. W. and H. Kloosterhuis, 1990, Data assimilation for non-linear tidal models, International Journal for Numerical Methods in Fluids, 11, 2, pp. 1097–1112.

Korres, G., M. Ntoumas, M. Potiris and G. Petihakis, 2014. Assimilating Ferry Box data into the Aegean Sea model. Journal of Marine Systems, 140 (2014) 59–72.

Korres, G., K. Nittis, L. Perivoliotis, K. Tsiaras, A. Papadopoulos, I. Hoteit and G. Triantafyllou, 2010. Forecasting the Aegean Sea hydrodynamics within the POSEIDON-II operational system. Journal of Operational Oceanography, Vol. 3, nu. 1, 37-49.

Korres, G., K. Nittis, I. Hoteit and G.Triantafyllou, 2009. A high resolution data assimilation system for the Aegean Sea hydrodynamics. Journal of Marine Systems, 77, 325-340.

Korres G. and A.Lascaratos, 2003. A one-way nested eddy resolving model of the Aegean and Levantine basins: Implementation and climatological runs. Analles Geophysicae, MFSPP – Part I Special Issue, 21, 205-220.

Langland, R.H. and N.L. Baker, 2004, Estimation of observation impact using the NRL atmospheric variational data assimilation adjoint system, Tellus, 56A, 189-201

Lekien, F., C. Coulliette, R. Bank and J. Marsden (2004), Open-boundary modal analysis: Interpolation, extrapolation and filtering, Journal of Geophysical Research, Vol. 109, C12004, doi: 10.1029/2004JC002323.

Liu, J. and E. Kalnay, 2008, Estimating observation impact without adjoint model in an ensemble Kalman filter, Quarterly Journal of the Royal Meteorological Society, Vol. 134, 634, 1327-1335

Luyten, P., 2011. COHERENS – A coupled Hydrodynamical-Ecological Model for Regional and Shelf Seas: User Documentation. Version 2.1.2, RBINS-MUMM Report, Royal Belgian Institute of Natural Sciences, 2011.

Madec, G. (2008). NEMO ocean engine.

Mellor, G. L., Häkkinen, S. M., Ezer, T., & Patchen, R. C. (2002). A generalization of a sigma coordinate ocean model and an intercomparison of model vertical grids. In *Ocean Forecasting* (pp. 55-72). Springer Berlin Heidelberg.

Papadopoulos, A., G. Kallos, P. Katsafados, S. Nickovic, 2002. The Poseidon weather forecasting system: an overview. Glob. Atmos. Ocean Sys., 8, 218-237.

Pasaric, M., & Orlic, M. (2004). Meteorological forcing of the Adriatic: present vs. projected climate conditions. *Geofizika, 21,* 69-87.

Pinardi, N. and G.Coppini, 2010.N. Operational oceanography in the Mediterranean Sea: the second stage of development. Ocean Sci., 6, 263-267.

Raicich, F. (1994). *Note on the flow rates of the Adriatic rivers* (Vol. 94, No. 8). Tech. Rep. RF 02.

She, J., B. Armstrup, K. Borenas, E. Buch, L. Funkquist, P. Luyten and R. Proctor: ODON: Optimal Design of Observational Networks, *Scientific report*, 2006.

Staneva, J., E. Stanev, J.-O. Wolff, T. H. Badewien, R. Reuter, B. Flemming, A. Bartholomae, and K. Bolding. “Hydrodynamics and Sediment Dynamics in the German Bight. A Focus on Observations and Numerical Modeling in the East Frisian Wadden Sea.” *Cont. Shelf Res.* 29 (2009): 302–19. doi:10.1016/j.csr.2008.01.006.

Stanev, E. V., Rahma Al-Nadhairi, Joanna Staneva, Johannes Schulz-Stellenfleth, and Arnoldo Valle-Levinson. “Tidal Wave Transformations in the German Bight.” *Ocean Dynamics* 64 (2014): 951–68. doi:10.1007/s10236-014-0733-6.

Stanev, E.V., F. Ziemer, J. Schulz-Stellenfleth, J. Seemann, J. Staneva, and K.W. Gurgel. “Blending Surface Currents from HF Radar Observations and Numerical Modelling: Tidal Hindcasts and Forecasts”, Accepted by J. Atm. And Ocean Technology, 2014.

Stewart, R.H., and J.W. Joy. “HF Radio Measurements of Surface Currents.” *Deep-Sea Research* 21 (1974): 1039–49.

Sumihar, J.H. and M. Verlaan, 2010: Observation sensitivity analysis, Developing tools to evaluate and improve monitoring networks, Deltares report no. 1200087-000, 35 pages.

Verlaan, M., A. Zijderveld, H. de Vries, and J. Kroos, 2005, Operational storm surge forecasting in the Netherlands: developments in the last decade. Phil. Trans. R. Soc. A, 363, No. 1831, 1441-1453.

Verlaan, M., N. van Velzen, S. Hummel, and H. Gerritsen, 2010, OpenDA, a generic toolbox for data assimilation in numerical modelling. Presented at JonsMod workshop May 2010.

Xie, P., & Arkin, P. A. (1997). Global precipitation: A 17-year monthly analysis based on gauge observations, satellite estimates, and numerical model outputs. *Bulletin of the American Meteorological Society, 78(11),* 2539-2558.

Zijl, F., M. Verlaan, and H. Gerritsen, 2012, Improved water level forecasting for the Northwest European Shelf and North Sea through direct modelling of tide, surge and non-linear interaction, Ocean Dynamics, July 2013, Vol. 63, Issue 7, pp 823-847, DOI 10.1007/s10236-013-0624-2.